Collinear fast-beam laser spectroscopy at ISAC

Thomas Elias Cocolios
110034858

Master of Science Candidate

Physics Department

McGill University

Montréal,Québec

2005-12

A thesis submitted to McGill University in partial fulfilment of the requirements of the degree of Master of Science

Your file Votre référence
ISBN: 978-0-494-24645-0
Our file Notre référence
ISBN: 978-0-494-24645-0

A Jacob Ryczywol,
pour m'avoir donné le goût à la science
au cours de ces trois années folles à Hochissik Park...

ACKNOWLEDGEMENTS

The production of such a great work cannot be completed without the extensive collaboration of many people and I would like to take the time to thank all of them individually. Although ten volumes would not suffice, I shall try to be thorough and concise and if anyone feels that they are not properly acknowledged here, the matter can be resolved over a pint... outside of TRIUMF.

I would like to thank

- My supervisor, Jonathan K. Lee, for giving me the opportunity to work for him on this experiment; all the members from our group at McGill, John Crawford for the continued weather updates, Fritz Buchinger for his contribution and Sidney Gulick for his work on the laser lock; David Rosner with whom I achieved most of the improvements to the lanthanum setup. I feel compelled to also thank all the members from the collaboration, starting with the spokesperson Hans Schüßler and also Hideki Iimura and Robert Thompson.
- Everybody from the Physics Department of McGill University for keeping the atmosphere high in colour during my year of study there, with a special thank to Paula Domingues without who any graduate student would be a lost soul in the McGill world of administrative insanity.
- TRIUMF for allowing me to perform my research in a mind-building environment; Jens Lassen who was the first to welcome me and guide me through the laboratory and whose guidance has remained throughout my work; Phil Levy for making me part of his research on fluorine which gave me hope when all other aspects of my research

were killing my morale; all the people who contributed to the design and successful assembly of the equipment, the Design Office, the McGill Physics machine shop, Mike McDonald, Mel Good, Geoff Wight, to mention only few; Renée Poutissou's Data Acquisition group for building the data acquisition system for the collinear fast-beam laser spectroscopy and guiding me through all my programming uncertainties; Jens Dilling for believing in me and my skills and introducing me to the right people at the right time.

- All the people with whom I could talk of matter beyond Physics as TRIUMF would not be complete without the side tracks from science; the other graduate students, the summer and co-op students, everybody who contributed to my birthday nitrogen ice cream, Alisa Dowling and all the people who attended the now-famous Friday socials and the amazing display of cooking skills presented there.
- Erika for sharing with me all those fun moments and being so attentive and listening during my highest and lowest times; my roommate Laura for enduring my cooking and music for so long; Nathalie for bringing an unbiased look at my work and helping me see the light.

A very special thank goes to Matthew Pearson whose continued care and attention for my work has given me a reference and a guidance; his knowledge on the subject as well as his ideas helped me go forward when I felt stuck at first sight and his British humour always kept my French arrogance at bay, although British soccer is still not as good as French soccer.

I finally want to thank all the people who contributed to my sanity outside the laboratory, Sensei Amber and all my Purple Dragon brothers and sisters, Ingrid, Urban Yarn, Myriam and all my friends and family.

A special thank goes to my parents for their financial support from the beginning of my B.Sc.; I know that not everybody has the chance to get that kind of support and I deeply thank them for allowing me to go through those five years worry free.

The last thanks go to the one and only person who slept with me every night of this work, always resting on the right book or the right piece of paper, asking for the door when I had just started typing a sentence or asking for attention when I needed concentration, ★ Alice ★, my dear and beloved cat.

ABSTRACT

Collinear fast-beam laser spectroscopy is a method of studying atomic and ionic hyperfine structure where a particle beam and a laser beam are superposed along the same line. Such a facility exists at ISAC, TRIUMF, Vancouver, BC, and was designed especially for polarising radioactive beams of alkali metals.

In order to produce polarised fluorine for the use in NMR, the hyperfine structure of the $3s\ ^4P_{5/2}$ and $3p\ ^4D_{7/2}$ states has to be known. The hyperfine coefficients for those two levels are measured for the first time to be $A = 2645.6(6)MHz$ and $A = 1565.6(4)MHz$ respectively. The $3p\ ^4D_{5/2}$ state is also studied to measure the metastable atom fraction and its hyperfine constant is measured to be $A = 1148(5)MHz$.

A study of lanthanum ions is also carried out. Spectra for the $6s^2\ ^1S_0$ to $5d6p\ ^3D_1^\circ$ transition are measured with stable ^{139}La to evaluate the sensitivity of the equipment and with radioactive ^{131}La for preliminary commissioning of the isotope shift study.

RÉSUMÉ

La spectroscopie par laser à géométrie collinéaire sur faisceau rapide permet l'étude de la structure hyperfine électronique des ions et des atomes par la superposition d'un faisceau de particules et d'un faisceau laser sur le même axe. Cette méthode est utilisée à ISAC, TRIUMF, Vancouver, C-B, où un dispositif permet de polariser des faisceaux alcalins radioactifs.

Afin de produire des faisceaux polarisés de fluore pour les besoins d'expérience de RMN, l'étude de la structure hyperfine des niveaux $3s$ $^4P_{5/2}$ et $3p$ $^4D_{7/2}$ est requise. Leurs constantes hyperfines ont été mesurées pour la première fois aux valeurs respectives de $A = 2645.6(6)MHz$ et $A = 1565.6(4)MHz$. Le niveau $3p$ $^4D_{5/2}$ a été étudié pour déterminer la portion du faisceau de particules qui occupe le niveau métastable et la valeur de sa constante hyperfine a été mesurée à $A = 1148(5)MHz$.

La transition entre les niveaux $6s^2$ $^1S_0$ et $5d6p$ $^3D_1^\circ$ des ions de lanthane a aussi été observée avec un faisceau stable de ^{139}La afin d'évaluer la sensibilité de l'équipement puis avec un faisceau radioactif de ^{131}La afin de démontrer la faisabilité d'étudier la chaîne isotopique du lanthane.

TABLE OF CONTENTS

LIST OF TABLES

LIST OF FIGURES

CHAPTER 1
Introduction

Collinear fast-beam laser spectroscopy is a method that yields a very accurate measurement of the hyperfine structure and isotope shift for elements that cannot be produced in large abundance such as radioactive nuclei. From these measurements the nuclear moments and the change in mean square charge radius between isotopes can be extracted.

Collinear laser fast-beam spectroscopy can also be used to optically polarise beams for use at nuclear magnetic resonance and nuclear quadrupole resonance experiments. Those experiments require polarised radioactive beams be delivered to them.

The Isotope Separator and ACcelerator facility at the TRI-University Meson Facility produces radioactive beams that are of interest to physicists for both spectroscopy study and polarised experiment work. A collinear fast-beam laser spectroscopy setup at this facility is therefore of great interest and was designed originally specifically for polarising alkali elements. Recently the interest over that apparatus expanded to polarising fluorine.

The interest in pure spectroscopy came later and was brought up to complement a study started at the Japanese Atomic Energy Research Institute, Tokai, Japan, on the lanthanum ions. Some modifications to the original setup need to be implemented to work with ions rather than neutral atoms. The laser systems also have to be adapted to reach the appropriate transitions.

The aim of the present work is to study the Polarizer beam line to ensure optimal operation with the upcoming experiments using it. First the

hyperfine structure of the polarisation levels of the stable isotope of fluorine needs to be studied in order to evaluate the feasibility of polarisation of the radioactive nuclei. Then the setup needs to be modified and studied with stable lanthanum to ensure that the isotope shift in the neutron deficient lanthanum isotope chain can be measured.

Although having different physical interests, both projects are similar; they both share the same equipment and both require equivalent analysis. The acquisition of hyperfine spectra is the basis of any analysis. The equipment is presented first with the specificities to each experiment and then the feasibility of both the fluorine and the lanthanum experiments is discussed.

CHAPTER 2
Atomic structures

2.1 The atom

The atom is classically described as a point-like core containing most of the mass, the nucleus, surrounded by a cloud of electrons to balance the charge. An ion is an atom for which the cloud has been disrupted by the addition or removal of one or more electrons.

The electrons in the cloud have definite energies quantified in levels. The lowest energy level for each electron is called the ground state and is the one of most probability. Some energy states have low decay probability; those are called metastable states and have typical half lives of several ms, usually losing their energy by means other than the emission of a photon, such as collision with rest molecules. The energy states above ground are called excited states and most last only for ns.

The study of atomic energy levels is atomic spectroscopy. The easiest levels to probe are those due to the outermost electron(s) in the cloud. A high resolution method used for atomic spectroscopy is collinear fast beam laser spectroscopy, described in chapter 3.

Not all transitions are allowed by quantum mechanics. Only those that satisfy basic selection rules can be observed. Those rules affect all the contributions to the angular momentum. The parity of the electron has to change; the total electron spin cannot change, $\Delta S = 0$; the electron's angular momentum changes, $\Delta L = 1$; it follows that the total electronic angular momentum can change, $\Delta J = 0, \pm 1$; finally its projection over the z-axis can change too, $\Delta M = 0, \pm 1$ depending on the excitation method.

Note that the $J = 0$ to $J = 0$ transition is not allowed; thus for $J = 0$, we have $\Delta J = 1$.

The nucleus is however not a point-like object. It has properties such as shape, charge distribution and spin. Those properties affect the energy levels with different strengths; some effects are large like the nuclear Coulomb field, some effects have a smaller impact, giving rise to properties like the hyperfine structure discussed in the following section.

2.2 Hyperfine structure

One of the interactions that could affect the electron cloud is the coupling of the total electron angular momentum $\vec{J}$ with the nuclear spin $\vec{I}$. The combined angular momentum is $\vec{F} = \vec{I} + \vec{J}$ and thus can take several eigenstates of value F, integral or half-integral by steps of 1, that obey the relation

$$|I - J| \leq F \leq I + J. \tag{2.1}$$

The set of states resulting from this interaction is called the *hyperfine structure* of the electronic level. Note that if either the nuclear spin or the electron angular momentum vanish, the level does not have this structure for F takes a single value.

The interaction between the nucleus and the electron cloud can be expanded into a series of moments [1]. Because of parity and time conservation those can only be 2^k-poles, electric for k even, magnetic for k odd. The zeroth pole is the electric monopole of basic Coulomb interaction from which the energy levels result. The other poles, magnetic dipole, electric quadrupole, magnetic octupole, electric hexadecapole, ... are perturbations to this interaction and induce the hyperfine structure. To lowest order, this effect is due to the magnetic dipole moment and the electric quadrupole moment, the other moments being negligible unless the

nucleus is extremely deformed. The deviation from the original electron energy level for different values of F is given by

$$\Delta E_F = \frac{K}{2} \cdot A + \frac{\frac{3}{2}K(K+1) - 2I(I+1)J(J+1)}{2I(2I-1)2J(2J-1)} \cdot B, \tag{2.2}$$

where the factors in front of A and B come from the angular coupling of $\vec{I}$ with $\vec{J}$. The quantity $K = F(F+1) - I(I+1) - J(J+1)$ is the cosine factor from that coupling, A contains the information relative to the magnetic dipole moment and B the information relative to the electric quadrupole moment,

$$A = \frac{\mu_I \cdot H_0}{IJ} \quad \text{and} \tag{2.3}$$

$$B = \frac{eQ|\phi_{ZZ}(0)|}{4}, \tag{2.4}$$

where μ_I is the magnetic moment, H_0 is the magnetic field created by the electron at the nucleus, Q is the quadrupole moment and $|\phi_{ZZ}(0)|$ is the electric field gradient at the origin from the motion of the electron in the cloud. An illustration of the different effects is shown in figure 2–1. The level is first split into I or J states, whichever of the two is the smallest, by the magnetic dipole interaction and then those different energy levels are shifted by the electric quadrupole interaction.

2.3 Isotope shifts

Along an isotopic chain the nucleus changes and therefore so does its interaction with the electrons. An example is the possible change of nuclear magnetic moment and therefore of hyperfine structure.

In general, the frequency of the transition from one level to another is different. This difference in transition is called the *isotope shift* [2].

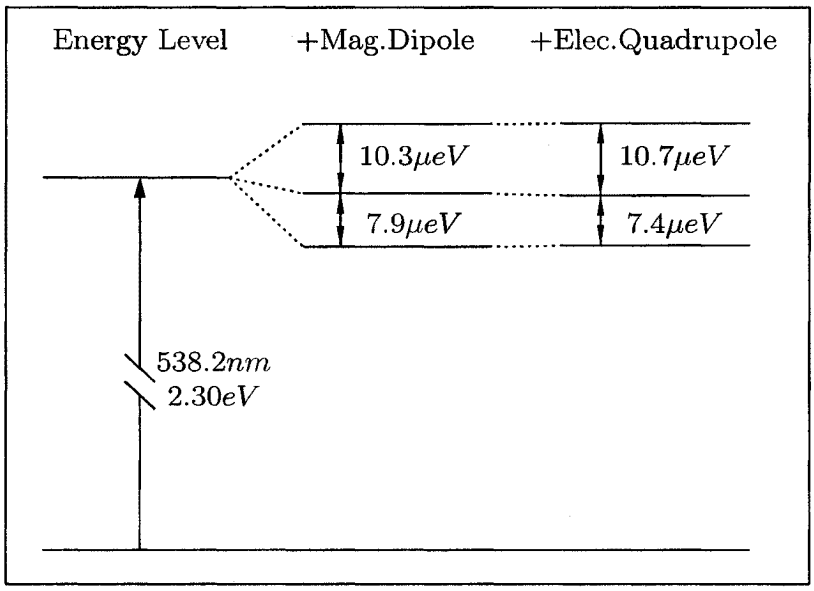

Figure 2–1: Hyperfine Structure of the $5d6p\,^3D_1$ level in ^{139}La in the scope of the $6s^2\ ^1S_0$ to $5d6p\ ^3D_1$ transition.

This change in transition energy has two distinct contributions, the mass shift $\delta\nu_{AA'}^{MS}$ and the field shift $\delta\nu_{AA'}^{FS}$ between two isotopes A and A':

$$\delta\nu_{AA'} = \delta\nu_{AA'}^{MS} + \delta\nu_{AA'}^{FS}. \tag{2.5}$$

2.3.1 Mass shift

The addition or removal of a neutron from one isotope to the next results in the change of the total mass of the nucleus. At each level, the difference in energy due to the mass variation is given by

$$\delta E_{AA'}^{MS} = \frac{m_{A'} - m_A}{m_A(m_{A'} + m_e)} \cdot \frac{1}{2}\left(\left\langle \sum_i \mathbf{p}_i^2 \right\rangle + \left\langle \sum_{i<j} 2\mathbf{p}_i \cdot \mathbf{p}_j \right\rangle\right), \tag{2.6}$$

where m_A and $m_{A'}$ are the masses of isotopes A and A' respectively, m_e is the mass of the electron and $\mathbf{p}_i$ and $\mathbf{p}_j$ are the electron momenta.

This shift occurs at both the base and the end levels of the electronic transition studied. The difference in change is thus to be considered. The

calculations at that point become quite complicated but in some cases, when the interaction between the electrons is reduced, the mass shift can be separated into two terms, one reflecting the change in Bohr radius of the studied electron, called Normal Mass Shift, and the change in the electron cloud, called the Specific Mass Shift.

As for the Normal Mass Shift $\delta\nu_{AA'}^{NMS}$, the reduced mass of the nucleus-electron system changes, therefore affecting the transition energy by

$$\delta\nu_{AA'}^{NMS} = \frac{m_{A'} - m_A}{m_A(m_{A'} + m_e)} \cdot m_e\nu, \tag{2.7}$$

where $\nu = \frac{\mathbf{p}^2}{\hbar m_e}$ is the frequency of the studied transition for isotope A.

The specific mass shift considers the interaction between electrons. As mentioned for the normal mass shift, the electron level scheme is directly affected by the change of mass of the nucleus. The interaction from electron to electron is not conserved and there is an overall change in the correlated interactions.

The general expression for the specific mass shift is

$$\delta\nu_{AA'}^{SMS} = \frac{m_{A'} - m_A}{m_A(m_{A'} + m_e)} \cdot \frac{1}{h} \left\langle \sum_{i<j} \mathbf{p}_i \cdot \mathbf{p}_j \right\rangle = \frac{m_{A'} - m_A}{m_A(m_{A'} + m_e)} \cdot K^{SMS}, \tag{2.8}$$

where K^{SMS} is independent of the isotope mass but only depends on the electronic structure. Unlike the Normal Mass Shift, the Specific Mass Shift cannot be calculated for large nuclei. Therefore, if one can extract the isotope shift information for the experiment, the Specific Mass Shift remains in the way of evaluating the Field Shift.

2.3.2 Field shift

The field shift is very different from the other effects for it is not caused by the change of mass of the nucleus but rather its change in volume.

The field shift is induced by the change of field interaction between the electron and the nucleus. As the nucleus gains or loses neutrons, its shape changes and so does the distribution of the charges within. It results in a change of the energy levels for the electron by

$$\delta\nu_{AA'}^{FS} = -\frac{Ze^2}{6\epsilon_0}\Delta|\Psi(0)|^2 \cdot \delta\left\langle r^2\right\rangle_{AA'}, \tag{2.9}$$

where Z is the number of protons, $\Delta|\Psi(0)|^2$ is the change in electron density at the nucleus between the lower and upper states in the transition and $\delta\left\langle r^2\right\rangle_{AA'}$ is the change in mean squared charge radius. This is the part of the isotope shift that has the most relevant information for the study of shape deformation along chain of isotopes through the study of the mean squared charge radius.

2.3.3 King plot

As mentioned in section 2.3.1, the specific mass shift cannot be calculated theoretically for complicated structures such as the rare earth elements. In order to extract the field shift information from the isotope shift, the two contributions – mass and field shift – have to be isolated, using a method called the King plot[3].

This analysis method uses the relation between pairs of isotopes whose isotope shifts are known to a reference pair of isotopes. First, the residual isotope shift $\delta\nu_{AA'}^{RIS}$ is calculated by removing the normal mass shift $\delta\nu_{AA'}^{NMS}$ from the isotope shift $\delta\nu_{AA'}$ pair by pair. The mass dependence of the specific mass shift is then removed by applying a modifying factor μ on the residual isotope shift that brings any pair to the same mass reference, as

$$\mu_{AA'} = \mu = \frac{(m_{A'} + m_e)(m_A + m_e)}{m_{A'} - m_A} \cdot \frac{m_{A'ref} - m_{Aref}}{(m_{A'ref} + m_e)(m_{Aref} + m_e)}. \tag{2.10}$$

Between two transitions labeled 1 and 2, since the isotope shifts are independent of the mass of the isotopes, the specific mass shifts are the same, namely $\delta\nu^{SMS}_{ArefA'ref}$, while the modified field shifts μF^1 and μF^2 are proportional one to the other. Altogether we get the linear relation

$$\mu\cdot\delta\nu^{RIS2}_{AA'} = \frac{F^2}{F^1}\cdot\mu\cdot\delta\nu^{RIS1}_{AA'} + \frac{m_{A'ref} - m_{Aref}}{(m_{A'ref} + m_e)(m_{Aref} + m_e)}\cdot\left(K^{SMS2} - \frac{F^2}{F^1}\cdot K^{SMS1}\right). \tag{2.11}$$

Plotting $\mu\cdot\delta\nu^{RIS2}_{AA'}$ as a function of $\mu\cdot\delta\nu^{RIS1}_{AA'}$ for each pair of isotope shifts between any two isotopes (A, A') should therefore yield a straight line with slope $\frac{F^2}{F^1}$.

In the case of a muonic transition, the interaction between the muon and the electron cloud is so small that the specific mass shift can be neglected. Using such a transition as a reference makes the analysis much easier. However, there are some cases in which such a study is not available and other techniques need to be considered, such as the X-ray spectroscopy from an inner shell electron, for which the specific mass shift is computable.

CHAPTER 3
Laser spectroscopy

As mentioned in chapter 2, the hyperfine structure of an atom is the result of the interaction between the nucleus and the atomic electron. Precision studies of this structure can therefore yield key information about the nuclear structure itself.

The basis of this work was set by Pauli in 1924 while interpreting observations from an experiment by Michelson [4]. The outermost electron of the atom was excited resonantly into a state of higher energy from which it decayed by spontaneous emission. The measurement of the light absorption as well as the collection of the reemitted light are the most fundamental observation methods for such spectroscopy.

The results were astonishing yet limited until the development of the laser in 1960 [5]. This revolution gave a new life to the study of atomic structure, giving access to higher resolution spectroscopy. The limiting factor with those new methods is the thermal distribution within the atom sample, inducing a Doppler broadening of the atom response to the excitation, as described in section 3.1.1.

The first response to this problem is to perform Doppler-free spectroscopy by creating a particle beam from an thermal source and collimating it to a single direction, while the spectroscopy is performed at 90° where the Doppler broadening is suppressed [6]. This method is very effective but requires a large sample for it is not very efficient, the interaction region being limited to the cross-point between the laser and the particle beam. This is therefore a method little used for radioactive atom study where samples are

limited to the small natural abundances, the natural decay of the samples or the production rates at appropriate facilities.

A way around that dilemma is the use of collinear fast-beam laser spectroscopy described later in this chapter in order to suppress the Doppler broadening.

3.1 Collinear fast-beam laser spectroscopy

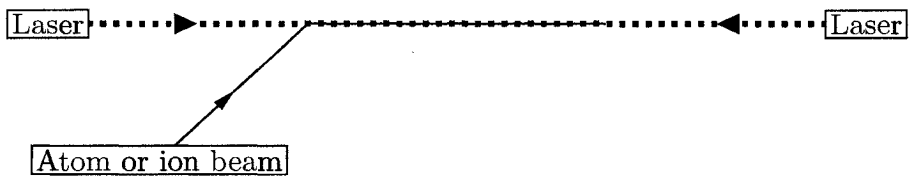

Figure 3–1: Fast-beam spectroscopy schematic. The solid line represents the atom or the ion path while the dashed line represents the laser path.

Collinear fast-beam laser spectroscopy consists of overlapping an accelerated atom or ion beam along with a laser beam, either counter- or co-propagating, as shown schematically on figure 3–1. Due to the motion of the particle beam the effective laser frequency is shifted according to the Doppler effect, expressed mathematically by

$$\nu = \nu_0 \cdot \sqrt{\frac{1-\beta}{1+\beta}}, \tag{3.1}$$

where ν is the frequency in the rest frame of the atom, ν_0 is the frequency of the laser in the laboratory frame and β is the velocity normalised to the speed of light in the direction of the laser beam. Note that if both the atom and laser beams are traveling in the same direction β is a positive quantity and the system is called *collinear* while if the two beams are propagating in opposite directions β is negative as per the laser beam and the system is

referred to as *contralinear*. The use of a post-acceleration region allows fine tuning of the Doppler effect and defines the region of observation.

Several techniques can be used to observe the atomic transitions, such as fluorescence detection or particle detection, yet all achieve high resolution thanks to a phenomenon called Doppler compression. The goal of all techniques is to produce resonance spectra.

3.1.1 Doppler compression

This is the main reason for using collinear fast-beam laser spectroscopy. The production of an atom beam, whether neutral or ionic, requires high operating temperatures for extraction and, if needed, ionisation. The result is a high thermal energy of the sample producing a Gaussian distribution ΔE of several eV width. The energy of the beam translates directly into velocity according to the kinetic energy formula, $K = \frac{1}{2}m\beta^2$, or, inversely

$$\beta = \sqrt{\frac{2K}{m}}, \tag{3.2}$$

where m is the mass of the particle.

It follows that there is a velocity distribution within the atoms, proportional to $\frac{\Delta E}{\sqrt{E}}$, as seen in figure 3–2, that leads to a distribution of the effective frequency given by equation 3.1, called Doppler width $\Delta\nu$. Expressed in terms of energy only, that distribution of effective frequencies is given by

$$\Delta\nu = \frac{\Delta E \cdot \nu_0}{\sqrt{2Em} \cdot (1 \mp \sqrt{\frac{2E}{m}}) \cdot \sqrt{1 - \frac{2E}{m}}}, \tag{3.3}$$

which gives, for $E << \frac{m}{2}$, a very steep curve, inversely proportional to the energy E. Hence, by raising the energy to several tens of keV, the distribution of velocities is greatly reduced, as seen in figure 3–2

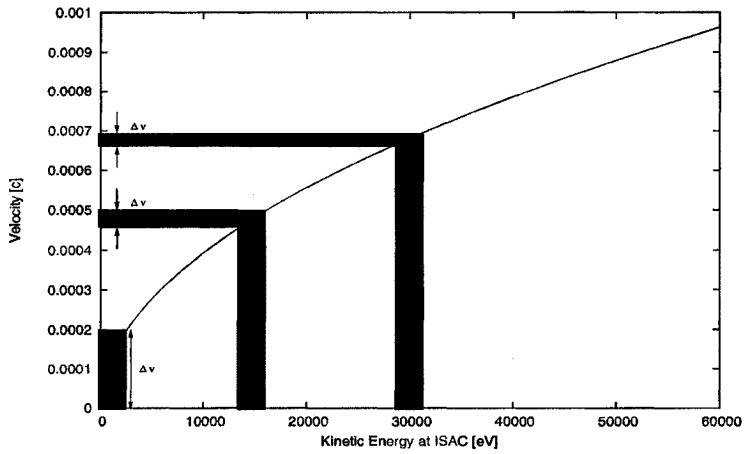

Figure 3–2: Reduction in velocity distribution by Doppler compression. The vertical boxes represent the same energy spread while the horizontal boxes represent the induced velocity spread of the particles at different particle beam velocities.

Table 3–1: Example of Doppler compression on ^{139}La-II ions at different energies assuming an initial energy spread of $\pm 3eV$ from the temperature distribution of the source for a transition at $538nm$.

Beam Energy [eV]	Frequency Spread [MHz]
3	5364
14156	55
30600	38

reducing the Doppler width of the peaks significantly. An example of such compression is given in table 3–1.

3.1.2 Frequency scanning

The excitation of an electron, as described in section 2.1, is limited in frequency space and is homogeneous. This gives rise to a Lorentzian distribution which is mixed with the inhomogeneous thermal distribution of the particles, as described in section 3.1.1, that is Gaussian. The convolution

of those two profiles is called a Voigt profile,[1] defined in this work as

$$V(x) = \frac{\Gamma}{2\sigma\pi^{\frac{3}{2}}} \cdot \int_{-\infty}^{\infty} \frac{e^{-\frac{y^2}{\sigma^2}}}{(x - \bar{x} - y)^2 + \frac{\Gamma^2}{4}} \cdot \mathrm{d}y, \tag{3.4}$$

where Γ is the Lorentzian natural distribution width, σ is the Gaussian source related distribution width and $\bar{x}$ is the centroid of the peak in frequency space.

Much information on the studied transition can be extracted from those parameters. Γ is related to the optical transition lifetime of the involved states,[2] σ gives information on the source operation while $\bar{x}$ has the information on the hyperfine structure. Finally, coupling the intensity of each peak of the hyperfine structure with the centroids gives the centroid of the transition, required to extract the isotope shift from one isotope to the next.

Resonance spectra are obtained by observing the reaction of the atoms at different laser frequencies ν. Using equation 3.1, we note that there are two ways of scanning the laser frequency in the atom frame, either by scanning the laser frequency ν_0 itself or by changing the beam velocity β.

Scanning the laser frequency ν_0 is the most direct way of scanning the effective frequency. The linearity of the scan on ν depends only on the linearity of the scan on ν_0 as equation 3.1 is exactly linear in ν_0. The typical range over which a tunable laser can be automatically scanned is $30GHz$, which is also a typical range for the hyperfine structure of an atom or an ion.

---

[1] see appendix A

[2] The ground state has an infinite atomic lifetime.

The problem with this method is the lack of reproducibility of such scans. Even if a single scan can be well performed and all the parameters recorded, its starting point and progression can not be reproduced, making statistical summation a complicated task if weak signals are to be expected, as discussed in section 5.3.3.

3.1.3 Doppler scanning

Scanning the beam energy at the post-acceleration region has the advantage that the laser system can be left untouched throughout the acquisition of the spectrum, thereby allowing the locking of the laser frequency for greater stability. The drawback is the non-linearity in energy. Although the effect is minor since $2K << m$, several kV on the post-acceleration electrodes are required to cover a range equivalent to a frequency scan from the laser.

3.2 Detection methods

In fast-beam collinear laser spectroscopy it is one thing to reach the proper frequency and excite the electron and another to observe that excitation. There are two different types of detection, direct fluorescence and particle detection, that can be used independently or combined.

3.2.1 Fluorescence detection

When the excited electron decays into a state of lower energy, a photon is released whose frequency corresponds to the energy difference ΔE between the two levels by the relation $\Delta E = h\nu$. Counting those photons gives an insight on the transition. This method is a direct observation of the interaction and therefore provides accurate information on the transition studied.

However, as this method is dependent on the direct observation of photons it has some inconveniences. First, the decay branches might be

of several types over a wide range of frequencies and the photon detector, usually a photomultiplier tube, has to work over that range. Then the laser light produces a background that has to be filtered out. If the decay transition is at the same frequency as the excitation the background from laser scatter can overwhelm the data; the use of the small difference in Doppler shift for photon traveling along the beam, as for the laser, or at an angle, like the emitted photons at 90°, can be a basis for scattered background filtering. In the case of different excitation and decay frequencies the suppression is much simpler thanks to the use of coloured filters.

In the end, each experiment is different from another and the special running conditions should be looked into case by case in section 3.3.

3.2.2 Particle detection

In the case of the migration of electronic population from one level to another, properties of the studied atoms can be used to observe a transition. A transition to populate – or depopulate – a metastable level can be used in an ionisation cell to get a variation in ion current from a neutral beam as ionisation cross sections are different. This method is used in this work as described in section 3.3.1.

The limits of such a method come from the strong dependence on the incoming beam current as well as from the dependence of the measurement on many external parameters such as the charge exchange cell efficiency and the particle counter used (Faraday cup, multichannel plate detector, ...)

Finally, the combination of particle and fluorescence detections through the use of coincidence measurement of the photons with the hit of a particle on a multichannel plate detector can help reduce the background, and thus the noise, by orders of magnitude [7]. Such techniques require low intensity

ion beams in order to properly identify the coincidence between the particle and fluorescence detections.

3.3 Polarizer beam line

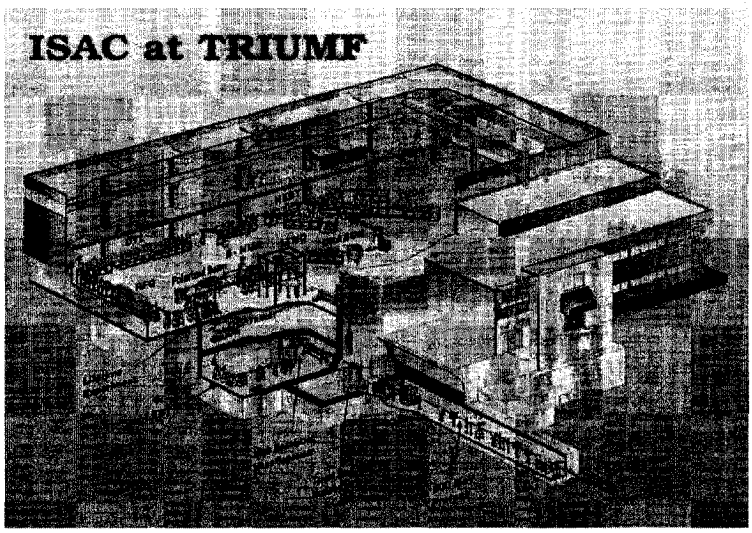

Figure 3–3: The ISAC facility at TRIUMF

The Isotope Separation and ACceleration (ISAC) facility at TRIUMF, is a radioactive beam facility. The proton beam from the main cyclotron is incident on a solid target. The isotopes produced are then ionised using one of various sources (surface ionisation, electron cyclotron resonance, laser resonance ionisation and soon FEBIAD) and accelerated to energies from $15keV$ to $60keV$. The produced beam is then separated according to mass-to-charge ratio using a high resolution bending magnet. The beam is finally delivered to various experiments sharing a large floor. Collinear fast-beam laser spectroscopy occurs on the polarized beam line shown in figure 3–3.

Although the ISAC facility is oriented toward providing radioactive beams it is possible to obtain stable beams from a parallel source, the Off-Line Ion Source (OLIS), that feeds the same beam line as ISAC. This is especially useful to probe the beam lines without risking contamination

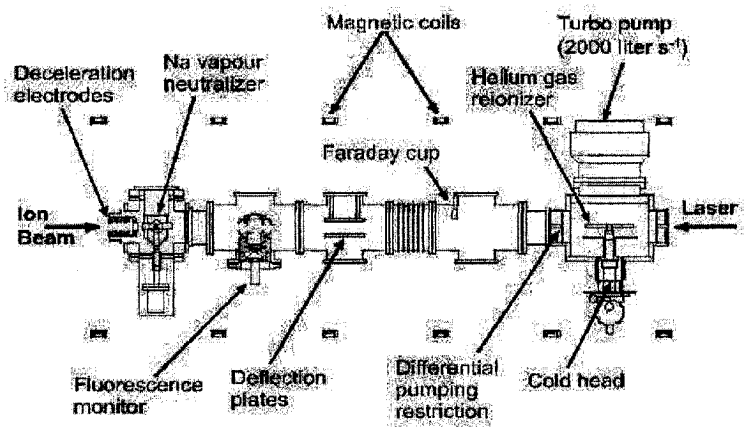

Figure 3–4: Polarizer beam line at ISAC

of the experimental hall. It also provides stable beams to test efficiencies and parameters of experiments and ensure the success of radioactive experiments. In the case of collinear fast beam laser spectroscopy OLIS provides a stable beam that is very useful for checking the performance of the overall apparatus as well as for preparatory study of the atomic fine and hyperfine structures of interesting atoms.

The Polarizer, as shown in figure 3–4, was first intended to provide polarised beams to experiments using NMR such as β-NMR or OSAKA. The polarisation is obtained by optically pumping in a weak magnetic field on a closed atomic transition using circularly polarised light. The Polarizer beam line requires some modifications to allow for laser spectroscopy on ions and those will be discussed in section 3.3.2. An overall schematic of the Polarizer beam line with all its components is also shown in figure 3–5.

3.3.1 Neutral beam

ISAC and OLIS provide the Polarizer beam line with an ion beam. In order to study the properties of the fluorine atom it first needs to be neutralised. This is the purpose of the Na charge exchange cell. After neutralisation any remaining ions are deflected away to work on the neutral

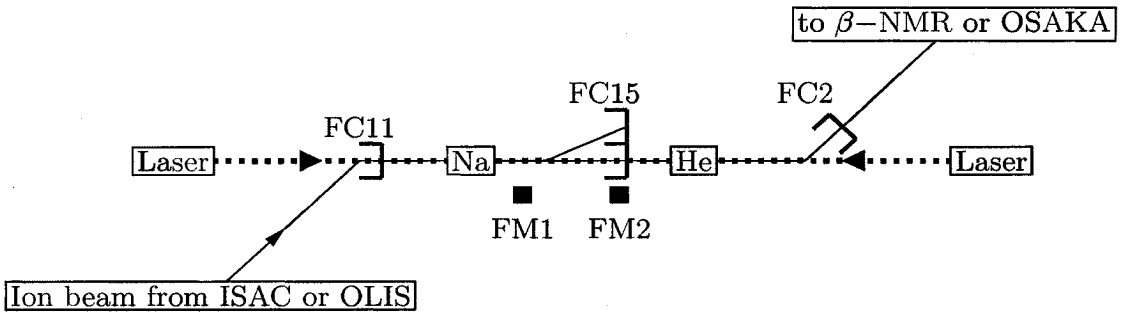

Figure 3–5: Polarizer beam line schematic. The solid line represents the atom or the ion path while the dashed line represents the laser path. FCs are the Faraday cups; FMs are the fluorescence monitors for photon counting; Na and He are the windowless cells for respectively neutralising and reionising the beam if studying the atom rather than the ion. Note that FC15 has two positions, in the beam or above it.

beam and reionise it through an impact ionisation He cell for further beam steering to experimental stations. Two detection methods can be used to measure atomic resonances in neutral beams, the induced fluorescence can be observed at both FM1 and FM2 or the difference in reionisation probability of different atomic states can be used for particle detection.

Post-acceleration electrodes

Collinear laser spectroscopy, as described in section 3.1, requires scanning a wide range of frequencies to observe all researched transitions. This is achieved in the Polarizer beam line by changing the energy of the ions as detailed in section 3.1.3. The beam energy is tuned using a series of post-acceleration plates in front of the Na cell. The exiting atoms keep their energy since they are not affected by electrostatic potentials.

The beam energy is scanned over a $1keV$ region using a scanning power supply controlled through the laboratory control system or using the system of power supplies described in section 3.3.2, depending on the experiment. The first method is of interest to set the system at an optimal value and monitor it in an integrated way in the laboratory while providing service to user experiments $\beta-$NMR and OSAKA, whereas the latter is meant to provide a quick response and high accuracy for hyperfine splitting study in preparatory work and fundamental studies.

Neutralisation and reionisation

The ions have to go through the Na neutralisation charge exchange cell first. The ions pass through a spray of Na vapour whose thickness is controlled by the temperatures of the reservoir and nozzle of the cell. The cell works by quasi-resonant charge-transfer reaction. The first step of any experiment with an atomic beam is therefore to optimise the Na cell temperature settings. Raising the temperature, and thus increasing the Na thickness increases the probability for the ions to neutralise, but it also increases the spread of energy of the beam. All those parameters have to be kept in mind to ensure optimal running conditions. The neutralisation process can give rise to ground state atoms as well as metastable state atoms; this is of great importance as the state to be studied for fluorine in chapter 4 is the metastable state $3s^4P_{5/2}$.

Once the work on the neutral beam is complete, the atoms need to be reionised in order to be transported to the experiments further downstream or for the purpose of particle detection. This is achieved through an impact ionisation cell filled with He. The higher the He density, the higher the reionisation probability however, the beam is scattered significantly at higher density. The density also influences the degree of preferential

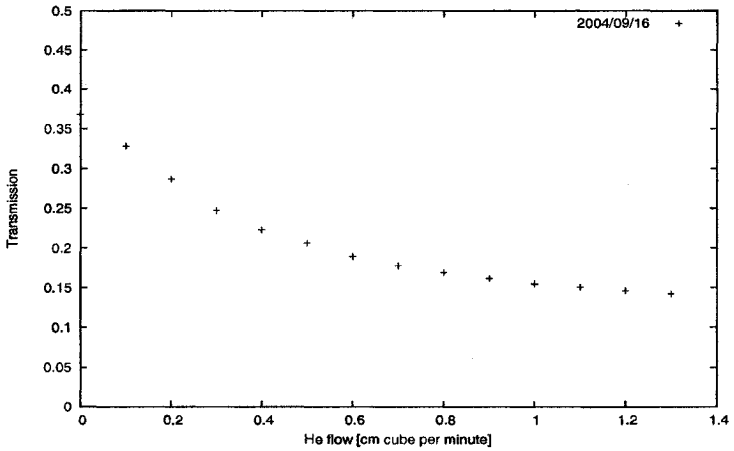

Figure 3–6: Transmission through the He cell for the fluorine beam.

ionisation, as discussed in section 4.5. The transmission through the He cell is measured by comparing the current on Faraday cup before the Polarizer beam line (FC11) to the current after the He cell at FC2 while the Na temperature is low enough to prevent neutralisation. The transmission t is then given by

$$t = \frac{FC2}{FC11}. \tag{3.5}$$

The transmission through the He cell is shown in figure 3–6.

Atom-ion separation

Every time the ionisation state of the beam is modified, the changes do not affect the whole beam. At neutralisation, some part of the beam is neutralised and the rest is left as ions; at reionisation, some of the neutral beam is reionised while the rest of the neutral beam is left neutral and flies through the He cell unaffected. Hence there are two steps at which the beam has to be purified.

The first step is to remove the ions from the neutral beam. This is accomplished using the deflector plates shown on figure 3–4 which are located between FM1 and FM2. The ion beam is dumped in FC15 in

its off-beam axis position while the neutral beam goes through. The neutralisation efficiency, comparing the current at FC11 to the neutral current, characterises the system. The neutralisation efficiency n is actually calculated using the left over part of the beam collected at FC15 and given by

$$n = 1 - \frac{FC15}{FC11}. \tag{3.6}$$

Due to the absence of focusing elements between the Na cell and FC15, the beam shape expands and the reading on FC15 can be inaccurate. There is therefore a need for normalisation of the currents. Assuming $n = 0$ when there is no Na, that is at low Na temperature T, the current at FC15 should be the same as at FC11. Hence the neutralisation efficiency becomes

$$n = 1 - \frac{FC15}{FC11} \cdot \left(\frac{FC11}{FC15}\right)_{lowT}, \tag{3.7}$$

where $(\frac{FC11}{FC15})_{lowT}$ is measured initially. The neutralisation efficiency is highly dependent on the Na cell temperature T, as shown in figure 3–7.

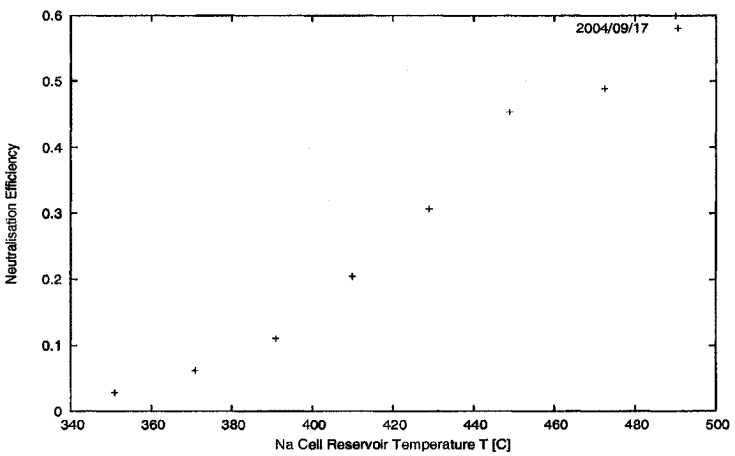

Figure 3–7: Neutralisation efficiency of the fluorine beam at the Na charge exchange cell

The other step at which it is required to split the atoms from the ions is after the reionisation process. This is achieved by turning the ion path toward FC2, using deflection plates, while the neutral atoms are dumped at the end of the straight section. If studying radioactive isotopes, the observation of the decay at the dump gives information on the reionisation efficiency. Otherwise the reionisation efficiency p can be calculated using

$$p = \frac{1}{nt} \cdot \frac{FC2}{FC11}. \tag{3.8}$$

The graph of the reionisation efficiency is shown in figure 3–8. Finally, the overall efficiency ϵ of the Polarizer is the comparison between the input and the output beam current while neutralising the beam at the Na cell and reionising it at the He cell. ϵ is given by

$$\epsilon = pnt = \frac{FC2}{FC11} \tag{3.9}$$

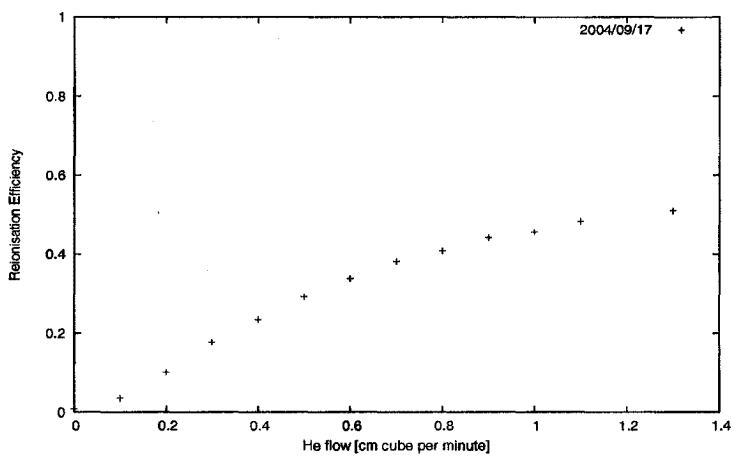

Figure 3–8: Reionisation efficiency of the fluorine beam at the He impact ionisation cell

Fluorescence detection

One of the methods for studying optical transitions is to observe the decay of the excited state created by the optical stimulation. The photons emitted by the decaying atoms are collected at a photomultiplier tube (PMT), Hamamatsu H7421-40, while the background photons, coming from stray light, laser scattering or scattering from gas atoms (Hühnermann leuchten), are suppressed using an Andover interference filter. The photons hitting the PMT are then counted using a scaler that is triggered by the acquisition system.

Two configurations are used during acquisition with this system. Two PMTs are placed in the Polarizer, called FM1 and FM2 on figure 3–5. Information on optical pumping and polarisation can be collected by comparing the signals from the two PMTs. However, for collinear laser spectroscopy, FM1 is the most interesting as it is the closest to the beginning of the interaction region and thus gives a response least affected by optical pumping. Therefore all hyperfine splitting information regarding collinear laser spectroscopy on fluorine using fluorescence detection is collected at FM1.

The fluorine transition studied in this work has a wavelength of $685.61nm$. The decay from the excited state is most probable through the same transition making it difficult to suppress the background coming from the laser scatter. However, since the emission from the excited state is looked at from an angle of 90°, the Doppler correction gives a difference of the order of $1nm$ in the wavelength. The narrow bandwidth interference filter then suppresses effectively the laser scattered background light.

Particle detection

The particle detection method aims at observing a change in the beam current. This is achieved thanks to preferential reionisation at the He cell. The neutral atoms in a metastable state are more likely to be reionised as their ionisation potential is reduced in comparison to the ground state atoms. It is therefore expected that, if that state would be emptied by optical pumping, the current after the He cell at FC2 would decrease. The transition used for that purpose is the $677.34nm$ transition from the metastable state to an excited state that decays to the ground state with high probability.

In order to measure the decrease in current with a good ratio of signal-to-noise a lock-in amplification method is used with the Faraday cup. The intensity of the laser light is modulated mechanically using a chopper wheel at a frequency of $1699Hz$; that signal is also used as a reference for a lock-in amplifier. The current from FC2 is fed directly to the input of the lock-in amplifier. When the energy is set at the resonant value for the transition the current at FC2 is modulated because of the laser optically pumping the transition away from the metastable state when exposed. Although this method does not give a direct measure of strength of the interaction, it gives as much information as the fluorescence detection method regarding the peak centroids, splittings and widths as will be discussed in chapter 4.

3.3.2 Ion beam

Although it is not its primary function, the Polarizer beam line can be used to study ion beams. If the temperature of the Na cell is kept low or if the Na is removed from the system there is no neutralisation taking place. As a consequence, the particle detection method as described in section 3.3.1 cannot be used and the study is limited to fluorescence detection.

Post-acceleration electrodes

If the post-acceleration electrodes of the neutral beam setup were used, the ions would regain their energy once out of the electrode field region and would not be at resonance in front of the fluorescence monitor. As a consequence, different post-acceleration electrodes had to be designed and placed in front of FM1. The core of that post-acceleration is a mesh set at the potential required to modify the ion energy. The use of a mesh ensures that the ions are under a constant potential while the mesh lets a high portion (60% to 85%) of the photons emitted pass through. The fringe effects at the entrance of the mesh are non-negligible. The peak shape could be greatly affected if the interaction is observed at a region where the field is not uniform. The initial mesh design is shown in figures 3–9 and 3–10.

An improvement to this original design is first to reduce the penetration of the external field inside the mesh. This is done by adding a reduced aperture at the entrance of the mesh. A second improvement to the mesh design is required to bring the ions gradually to the right potential rather than through a sudden jump. This is achieved by having a series of 4 plates going from ground to the right potential using a voltage divider to set each plate at an intermediate step. For tuning purposes a plate segmented into four quadrants was added at the front of the post-acceleration electrodes. Those quadrants are connected to virtual grounds and by reading the current on each of them the beam can be positioned and then adjusted to go through the center of the mesh. For symmetry purposes and to ensure the beam quality is not too seriously affected, the post-acceleration electrodes are made symmetric. The design of that second stage post-acceleration system is shown in figures 3–11 and 3–12.

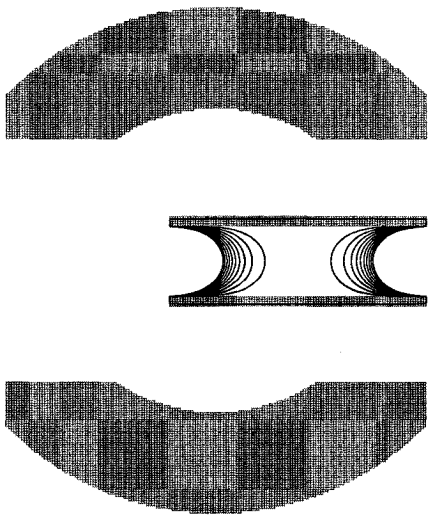

Figure 3–9: SimIon representation of the mesh in first stage; the field lines are for every 0.1% of the set value from 99% to 99.9%.

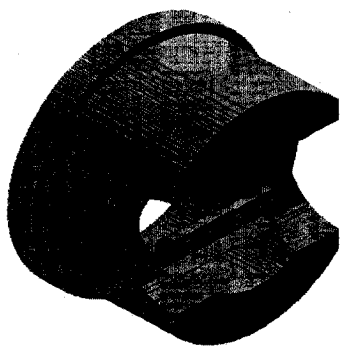

Figure 3–10: SimIon 3-dimensional representation of the mesh in first stage. Only the fluorescence monitor half side is represented.

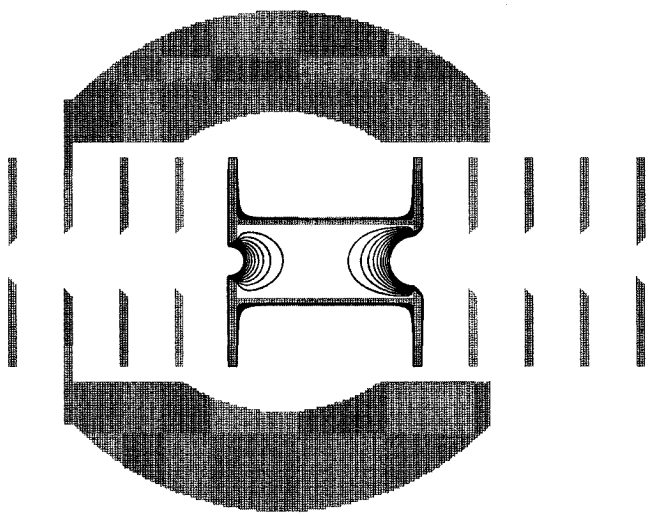

Figure 3–11: SimIon representation of the mesh in second stage; the field lines are for every 0.1% of the set value from 99% to 99.9%.

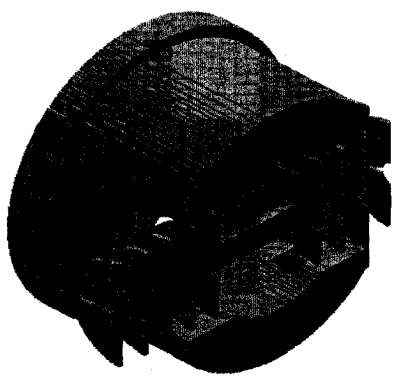

Figure 3–12: SimIon 3-dimensional representation of the mesh in second stage. Only the fluorescence monitor half side is represented.

The bias on the mesh in any design is provided by two power supplies; a scanning Kepco BOP 1000M power supply operates as a $\times 100$ amplifier for a $-10V$ to $10V$ input to provide a scanning range from $-1kV$ to $1kV$ and float the Harrison 6516A power supply. The Harrison supply adds a constant step between $0V$ and $3kV$ and can be used with either polarity. The overall potential that can be applied with this setup therefore ranges between $-4kV$ and $+4kV$.

The output is monitored by a 1000 : 1 divider which is read by a precision ADC and recorded during acquisition. It is then sent to the mesh in the original setup or a divider in the second design so as to provide the potential to the intermediate stages of the post-acceleration. The stability of the output and its relevance for the study of collinear laser spectroscopy is discussed in section 5.4.

Fluorescence detection

Collinear laser spectroscopy with the ions is performed in front of FM1, shown right after the Na cell in figure 3–5. It observes the decay of the excited ions in the mesh electrode shown in figure 3–12 in the large opening on the side.

The photons are collected with a lens and a mirror for a total collection that is discussed in section 5.3.3. The background is filtered with glass filters as the main decay branch frequency is different from the laser frequency, as also discussed in the section 5.3.3.

3.4 Lasers

The two collinear laser spectroscopy experiments studied in this work operate at different laser frequencies, therefore requiring different laser systems.

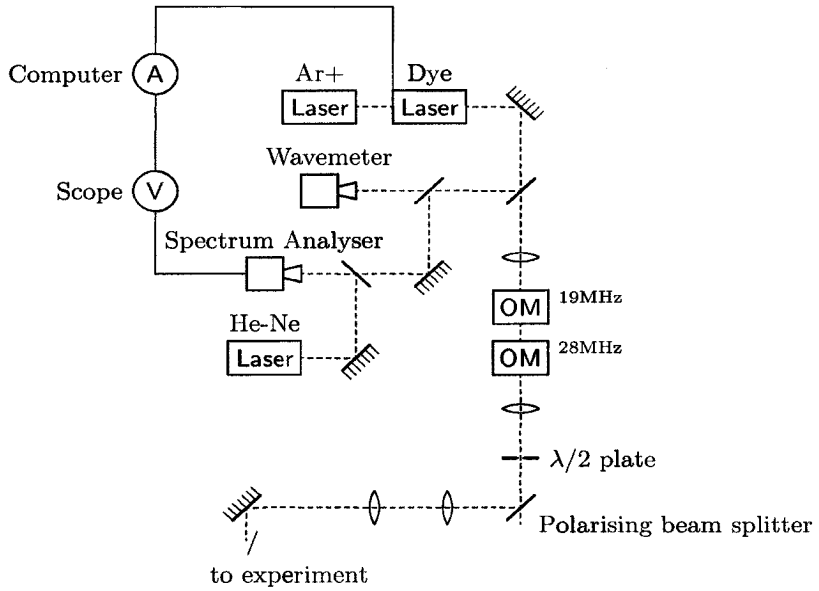

Figure 3–13: Polarisation laser system. The dashed line represents the optical path while the solid line represents the electrical connections.

3.4.1 Polarisation lasers

A Coherent Innova 200 Ar^+ laser pumps a Coherent 899 ring dye laser to produce the range of frequencies of interest. The dye used for the fluorine study performed with this laser system is DCM. With a pump power of $6W$ it provides up to $200mW$ of power at the desired frequency.

The output of the dye laser is monitored with a wavemeter to measure its frequency and also with a spectrum analyser that compares the laser beam to a frequency stabilised0 $He - Ne$ line. The spectrum analyser provides a feedback to the dye laser to correct any drift of the laser over long periods of time. The output of the dye laser is therefore known to be very stable, although the accuracy of its absolute value is conservatively estimated to be $\pm 100MHz$ on the wavemeter calibration.

The output, prior to be used in the Polarizer beam line, can be broadened using two electro-optical modulators (EOM) at $19MHz$ and $28MHz$

that provide sidebands to the laser frequency spectrum in order to reach a greater number of atoms. The improvement of the interaction strength is about 50%. However, it complicates the peak shape. Those are therefore not used for precision spectroscopy but rather for efficient polarisation or metastable depopulation.

The laser beam is finally polarised appropriately through a $\lambda/2$ plate to be sent to the experiment through the polarised beam splitter. Modifications to that system will be needed for polarising ^{20}F and that is discussed in section 4.6.

3.4.2 Spectroscopy lasers

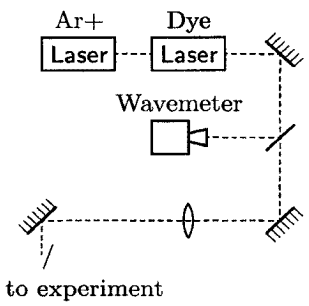

Figure 3–14: Spectroscopy laser setup. The dashed line represents the optical path.

The collinear spectroscopy setup for the study of lanthanum requires a laser that provides a wavelength about $538nm$. Therefore a Coherent Innova 100 Ar^+ laser pumps a Coherent 699-21 ring dye laser with Rhodamine 110 dye.

Typical operating conditions are to pump the dye with $6.3W$ at $514nm$, which gives an output from 30 to $150mW$ from the dye laser in single frequency mode. The power output depends greatly on the frequency required and unfortunately this experiment runs on the limit of the dye

range. However, the power output should be sufficient to saturate the transition. This effect will be discussed in section 5.3.2.

The frequency of the output is monitored at a wavemeter with accuracy $\pm 900 MHz$. Finally the beam is transported to the interaction region by mirrors and a single long focal length lens, as seen on figure 3–14, and enters the evacuated beam line through a window.

There is no frequency lock for that setup in its original configuration and the frequency may drift at an average rate of $\pm 250 MHz$ per hour. This issue is discussed in section 5.4.2 and concludes on the recent development of a laser frequency lock for this laser setup, described in appendix C.

The laser beam produced by the dye laser has a diverging Gaussian spatial power distribution to its power and this distribution expands in space. If the laser beam is left untouched, its size at the interaction region after transport is extrapolated from beam size measurements along its transport path. This measurement is carried out by monitoring the power drop as a knife-edge on a translation mount reduces the laser light transmitted to a photomultiplier. The beam size measurements and its extrapolation are shown in figure 3–15. The implementation of two lenses for beam focusing along the transport line can reduce the laser beam radius at the interaction region from over $5mm$ to below $2mm$. The radius of the smallest aperture of the post-acceleration electrodes is $4mm$ and it is therefore required to have a laser beam that fits well within it so as to minimise laser scatter.

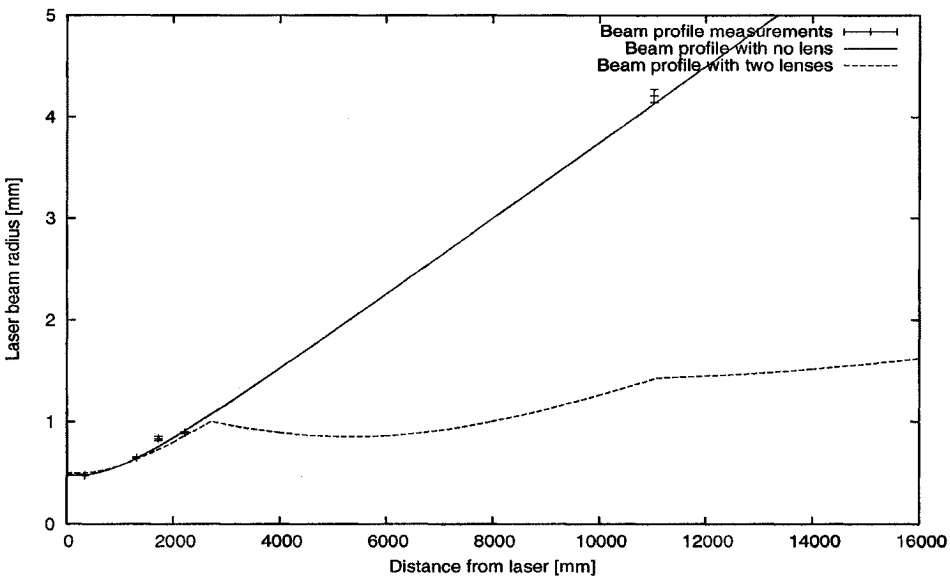

Figure 3–15: Spectroscopy laser beam natural profile if not affected by any reshaping element. The size of the beam is defined at the $1/e^2$ power drop radius. The lenses used for the reshaped beam profile are $f = 2500mm$ and $f = 10000mm$, using Gaussian beam optics calculations [8].

CHAPTER 4
Feasibility of polarising fluorine

The OSAKA-Minamisono group at ISAC wishes to use nuclear magnetic resonance (NMR) to extend their work on ^{20}Na to its mirror nucleus ^{20}F. In order to do so they require a polarised ^{20}F beam. The polarisation of fluorine requires cycling the neutral atom from the metastable $3s\ ^4P_{5/2}$ state to the excited $3p\ ^4D_{7/2}$ state through the use of optical pumping with circularly polarised light on the closed $685.60nm$ transition while defining the polarisation axis with a weak magnetic field. As a preliminary study the hyperfine splittings of the metastable and excited states need to be measured in order to determine what laser frequencies are required to pump all the atoms. Moreover one wants to know what fraction of the population is in the metastable state and can be polarised.

4.1 Atomic structure of fluorine

Fluorine atomic structure is one electron short of a closed shell, making this atom a single-hole structure. A valence electron requires a large amount of energy for excitation from the atomic ground state, $2s^22p^5\ ^2P^\circ_{3/2}$,necessary for carrying out optical pumping and polarisation of ground state atoms in a system that is most stable when the hole is filled. Any such excitation is carried by a high-frequency photon in the deep UV light range beyond the range of available lasers.

The solution to this challenge is to start from a metastable state that is already very high in energy and then polarise the beam. The state of interest for fluorine is $3s\ ^4P_{5/2}$, that has a lifetime of $3.7 \pm 0.5\mu s$[9]. From

that level the cycling transition at $685.60nm$ shown in figure 4–1 can be used to polarise the beam.

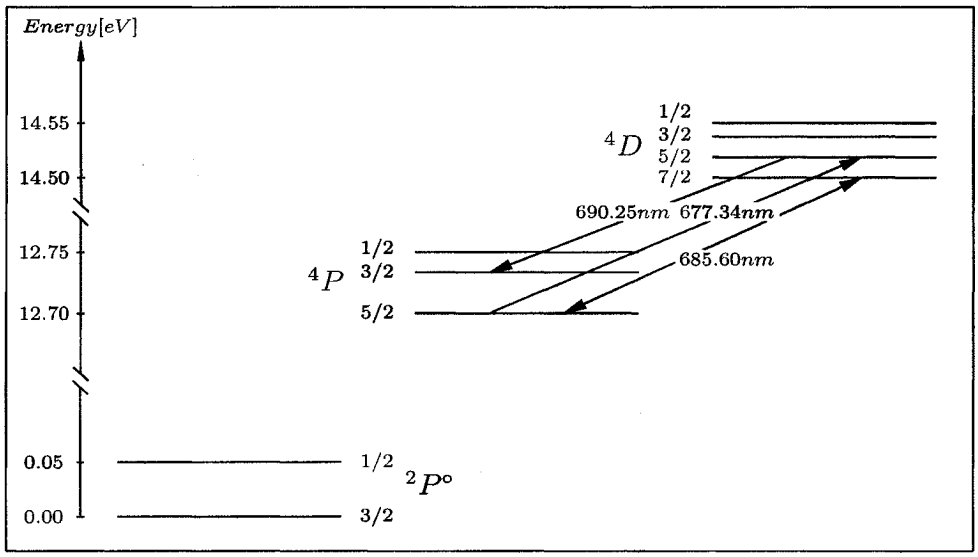

Figure 4–1: Fluorine atomic structure. Only the levels relevant to the polarisation of fluorine are represented on this drawing.

The metastable state is created during neutralisation in the Na vapour as described in section 3.3.1. As the atom cascades down through the structure, it has a chance of ending its decay in this metastable state. The time the neutral $40800eV$ atoms spend in the Polarizer beam line between the charge exchange cell and the reionisation chamber is similar to the metastable lifetime, leading to some loss in the metastable population during the optical pumping process.

Another level of interest is the fine structure component of the excited $3p\ ^4D_{5/2}$ level, because it can decay into the $3p\ ^4P_{3/2}$ state that rapidly decays to the ground state. Exciting the metastable atom into the $^4D_{5/2}$ state will ultimately depopulate the metastable state. The study of the $677.34nm$ transition therefore yields information on the fraction of metastable atoms

produced at the Na charge exchange cell, as explained in section 4.6, and thus on the polarisable fraction of the beam.

4.2 Studied beam

The preliminary study of polarising fluorine was performed on the stable isotope. A beam of $^{19}F^{+}$ is produced in the Microwave OffLine Ion Source (OLIS) using CF_4 gas. The beam is accelerated through a potential $40806V \pm 1\%$. This value will be discussed in section 4.3. The beam is then transported to the Polarizer beam line, described in section 3.3.1.

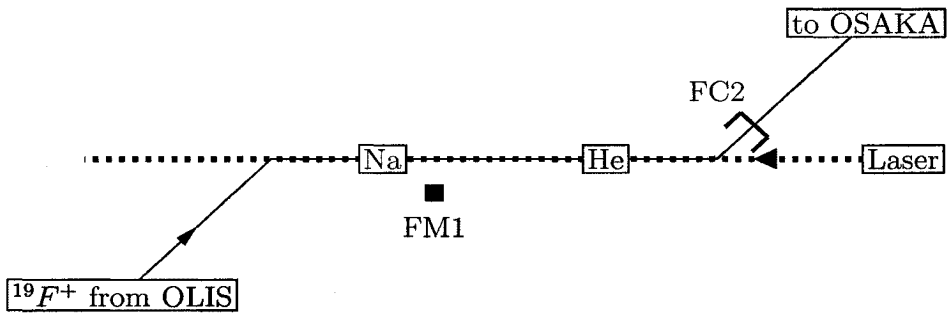

Figure 4–2: Schematic of the Polarizer beam line for the fluorine study. The solid line represents the fluorine beam while the dash line represents the laser beam. FC2 refers to the Faraday cup and FM1 is Fluorescence Monitor 1. Na and He are the windowless cells for respectively neutralising and reionising the fluorine beam.

The beam is neutralised in the Na vapour charge exchange cell and reionised in the He gas cell. On the opposite side, the laser is sent in the line using the setup described in section 3.4.1. The laser interaction of interest occurs with the neutral fluorine atoms between the two cells. Data

of this interaction are collected at the fluorescence monitor FM1 and at the Faraday cup FC2, as shown on figure 4–2.

4.3 Energy calibration

If one desires to achieve great precision in evaluating the hyperfine splittings, a great deal of care has to be taken in the experimental conditions to ensure that no factor is left clouded in the process. The hyperfine splitting refers to the difference between two frequencies and thus one would expect many measurement errors to cancel out. However, uncertainty in knowledge of the beam energy leads to a systematic error in the hyperfine splitting.

The uncertainty on the high voltage power supplies used by OLIS, as mentioned in section 4.2, is $\pm 1\%$, which gives an uncertainty of $\pm 400V$. The resulting uncertainty in splitting is then above $5MHz$ and could be up to $50MHz$ depending on the transition.[1] Hence the first step of any analysis must be the calibration of the source energy. This could be done using a well known transition together with great accuracy on the laser frequency. Note that this calibration is required for any type of collinear fast-beam laser spectroscopy and shall be discussed for lanthanum in chapter 5.

The first step is to fit the data with independent position parameters for each hyperfine resonance to evaluate the position of each independent peak, regardless of expected frequency splittings. Those channels are then averaged, weighted to the theoretical heights of the respective peaks as given by Clebsch-Gordan coefficients, giving the centre of gravity for the transition, also called centroid, in channel space. The centroid V_{cog} is

[1] see appendix B.

then translated into energy units using the least squares affine fit on the channel-to-readback data for the post-acceleration power supplies.

The second step is to evaluate the centroid energy from the transition and laser frequencies. Starting from the Doppler shift equation 3.1, where ν is the transition frequency, f is the laser frequency and m is the mass of the element, the equation can be reversed to give the energy

$$E = \frac{m}{2} \cdot \left(\frac{\nu^2 - f^2}{\nu^2 + f^2} \right)^2 + V_{cog}. \tag{4.1}$$

This greatly improves the accuracy of the beam energy. Smaller errors are contributed by the transition frequency, the laser frequency and the centroid of the spectrum.

The transition frequencies used in the different analyses are taken from the literature and had uncertainties ranging from $\pm 13Hz$ to $\pm 50MHz$ depending on the element and the transition, leading to very small errors in the hyperfine splitting.

The laser frequency uncertainty is a greater concern. The polarisation laser system drift is minimum by locking as described in section 3.4.1; however the uncalibrated wavemeter leaves room for a systematic frequency uncertainty that is evaluated conservatively to be $\pm 100MHz$. Again this contributes very little error to the hyperfine splitting.

Altogether the uncertainties add up to $10eV$ on the beam energy, which is clearly better than the power supply confidence value.

4.4 ^{19}F hyperfine structure

^{19}F has a nuclear spin of 1/2. The hyperfine structure of any state can therefore have up to two components making the hyperfine structure study relatively fairly simple. The metastable state of interest comprises two levels with $F = 2$ and $F = 3$ total angular momenta. Note that the excited states

will have a structure too, giving up to four different contributions to a single transition.

The transitions are identified through their relative intensities. Although the theoretical intensities as used for the energy calibration in section 4.3 are not quite reproduced due to external contributions such as metastable loss, the order of heights is kept and permits the identification of the peaks. Any other calculation is based on this initial identification.

The quadrupole moment is 0 for any $I = 1/2$ nucleus; therefore only the dipole moment is of interest for ^{19}F. The A coefficients for the different levels are extracted from spectra and then the information provided is used to deduce the hyperfine structure of ^{20}F.

4.4.1 Polarising transition

The spectrum from the $^4P_{5/2}$ to $^4D_{7/2}$ transition shown in figure 4–4 is obtained by direct observation of the fluorescence from the excited state as described in section 3.3.2. With the high beam current the output from the photomultiplier approaches saturation. This is taken into account while fitting the spectrum by discarding all points above a threshold set conservatively at $100kHz$.

The spectrum is acquired by stepping the potential on the deceleration electrodes as described in section 3.3.2. The data are recorded with respect to DAC channel numbers and not real potential. The first step of the analysis is to evaluate the correspondence between channels and voltages. The readback from the applied voltage is recorded at each channel, but as this value has an uncertainty of its own, it proves rather complicated to fit the spectrum as signal against readback. An alternative is to fit both the signal and the readback with respect to the DAC channels and then combine the two fits as follows.

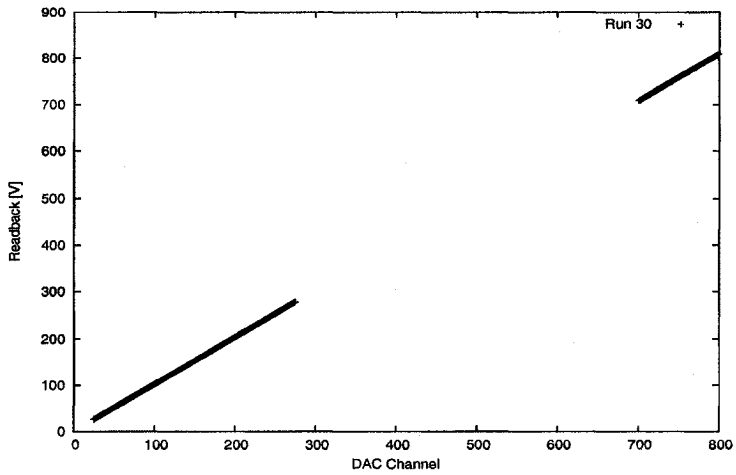

Figure 4–3: Voltage ramp from Run 30. The scan was performed in two separate sections to save time where no peaks were expected.

The channel-readback correspondence is evaluated. The contribution to the potential is of two types, the offset from the constant voltage power supply and the linear conversation factor from the ramping power supply. The resulting correspondence is a linear relationship as can be seen in figure 4–3.

The energy of the beam is then calibrated as described in section 4.3. The spectrum is finally fitted in frequency space to extract the A coefficients at once using a function made of the superposition of the background and as many peaks as required. For the present transition, three Voigt profiles were used for which the mean $\bar{x}$ from equation 3.4 contains equation 2.2 with the appropriate angular factors to each peak. Figure 4–4 shows the fit that this function produced.

The measured coefficients over all the spectra are averaged for improved precision and the final values are given in table 4–1. Those values will be needed to determine the polarisation scheme for ^{20}F in section 4.6.

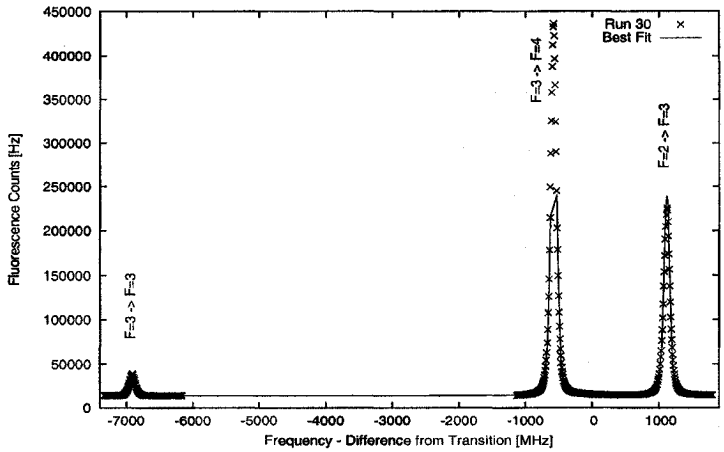

Figure 4–4: Hyperfine structure spectrum of the polarising $^4P_{5/2}$ to $^4D_{7/2}$ transition. On the middle peak, the fit is only performed for points below a threshold as the photomultiplier is reaching saturation above that level.

Table 4–1: Hyperfine A constants of the $^4P_{5/2}$ and $^4D_{7/2}$ states.

Level	$A\ [MHz]$
$^4D_{7/2}$	1565.6 ± 0.4
$^4P_{5/2}$	2645.6 ± 0.6

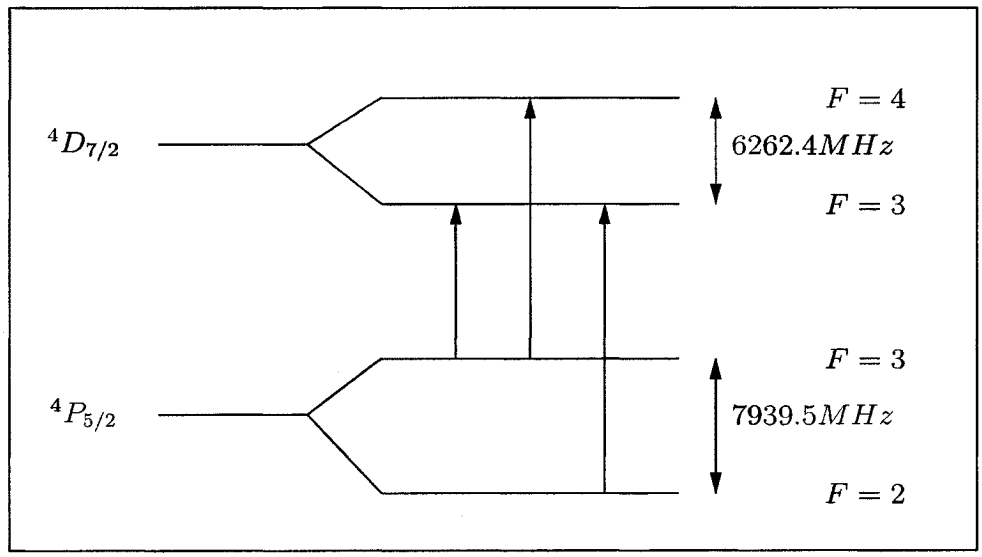

Figure 4–5: Hyperfine structure of the polarising transition in stable fluorine. Note that the diagram is not to scale.

4.4.2 Depopulating transition

Unlike the polarising transition described in section 4.4.1, the depopulating transition $^4D_{5/2}$ to $^4P_{5/2}$ is studied through particle detection as described in section 3.3.1. The output of the lock-in amplifier is fed into a voltage-to-frequency converter (VFC) that is connected to a scaler to integrate the counts.

One of the spectra obtained is shown in figure 4–6. The Kepco power supply has insufficient range to permit the observation of the whole structure in a single sweep. The spectrum shown in this work is the combination of two sweeps very close in time (within less than thirty minutes) to produce a complete structure. The analysis is done from this combined set, using the same method as in section 4.4.1 for the energy calibration. The interaction occurs all along the Polarizer beam line; the integrated time of the interaction is therefore greatly superior to the natural lifetime of the excited state. There is no contribution from a homogeneous distribution. It follows that the peak shape is purely Gaussian.

The A coefficients are extracted in the same way as with the polarising transition. The final values are shown in table 4–2. The error is much higher than for the $^4P_{5/2}$ to $^4D_{7/2}$ case due to the lower signal-to-noise ratio.

4.5 Metastable population

It is only possible to polarise the atoms that are in the metastable level. It is therefore of major importance to know what fraction of the beam is in that state. The neutralisation potential for the metastable state of fluorine is very close to the sodium ionisation potential. Therefore there is a quasi-resonant process that goes on enhancing the metastable population fraction. However, it is still required to investigate the size of this population.

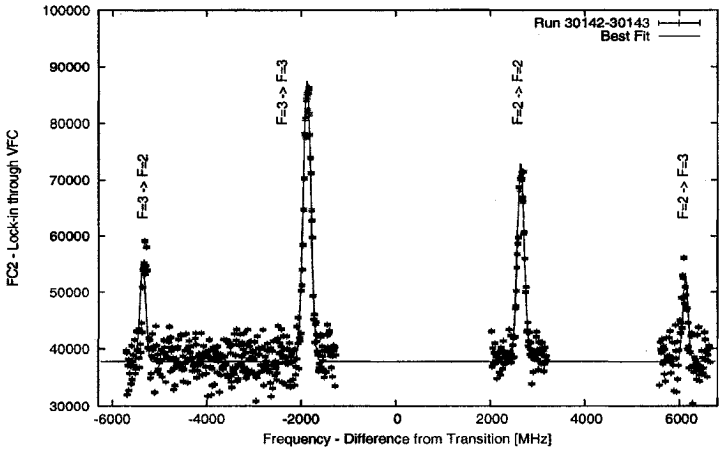

Figure 4–6: Hyperfine structure spectrum of the depopulating $^4P_{5/2}$ to $^4D_{5/2}$ transition.

Table 4–2: Hyperfine A constants of the $^4P_{5/2}$ and $^4D_{5/2}$ states.

Level	$A\ [MHz]$
$^4D_{5/2}$	1148 ± 5
$^4P_{5/2}$	2642 ± 5

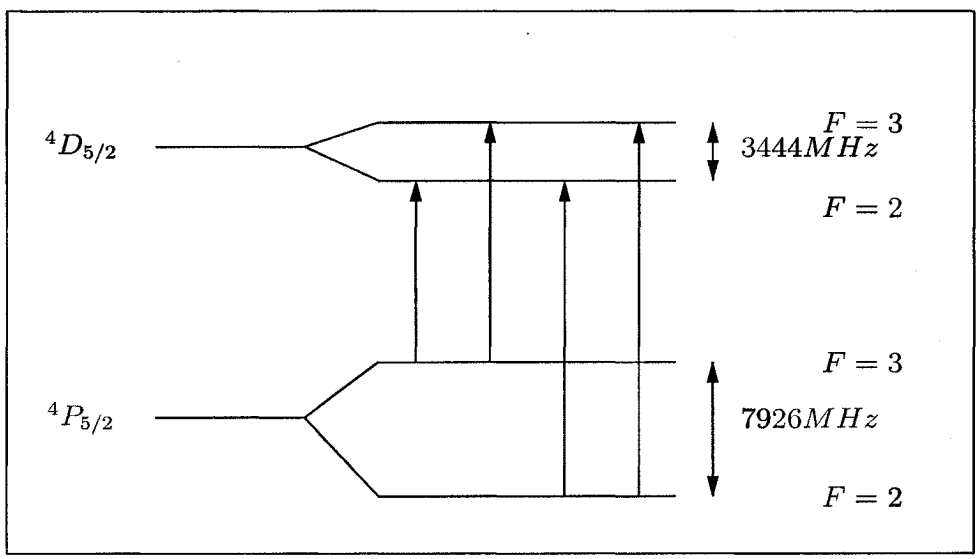

Figure 4–7: Hyperfine structure for the depopulating transition in stable fluorine. Note that the diagram is not to scale.

Labeling the fraction of metastable atoms f^* and the ground state atoms f, it is assumed that no other states are produced and therefore

$$f + f^* = 1. \tag{4.2}$$

It follows that the ion current I^+_{Off} after the reionisation cell, considering the population fractions as produced at the Na cell for the neutral beam I, is

$$I^+_{Off} = I \cdot [f^*(1 - e^{-A\sigma\pi}) + f(1 - e^{-\sigma\pi})], \tag{4.3}$$

where $\sigma\pi$ gives the ionisation efficiency and depends on the He pressure, directly related to the He flow, and $A = 3.4$ is the preferential ionisation factor. At low He flow it is expected that the ion current be very small and therefore a linear approximation can be made of the exponential factors so that

$$I^+_{Off} = I \cdot \sigma\pi[f^*A + f]. \tag{4.4}$$

As the laser beam is sent through the line at resonance with the depopulating transition, there is a migration in the population fraction. It is then reasonable to assume that half the population is transferred, considering only the strongest hyperfine transition ($F = 3$ to $F = 3$) is used. Equation 4.4 can then be rewritten for the new ion current I^+_{On} as

$$I^+_{On} = I \cdot \sigma\pi\left[f^*\left(\frac{A}{2} + \frac{1}{2}\right) + f\right] \tag{4.5}$$

since the new metastable population at reionisation is then $\frac{f^*}{2}$ and the ground state population becomes $f + \frac{f^*}{2}$.

The ratio of the two is then free from the ionisation parameters and only dependent on the population fractions and the preferential factor A. Moreover, from equation 4.2 we can write that $f = 1 - f^*$ from which we can reduce the ratio to be only a function of the metastable population fraction,

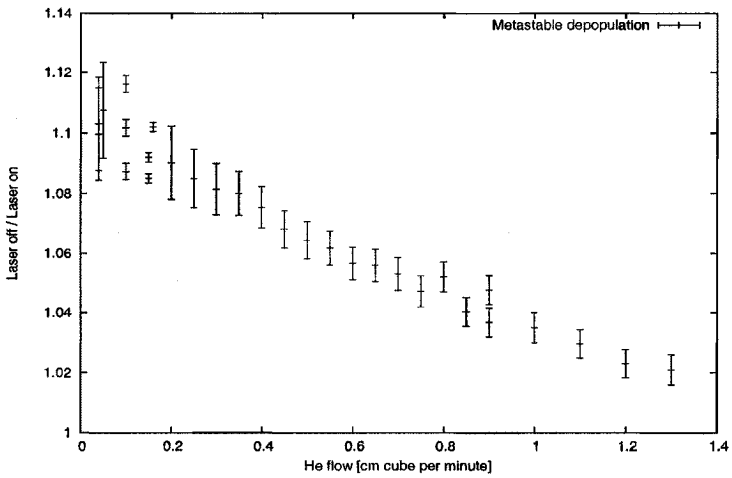

Figure 4–8: Preferential ionisation against He flow rate. The current at FC2 is measured with no laser and therefore original population fractions and with the laser set on the depopulating transition to modify the population fractions.

as

$$\frac{I^+_{Off}}{I^+_{On}} = 2 \cdot \frac{1 + f^*(A-1)}{2 + f^*(A-1)}. \tag{4.6}$$

In this approximation $\frac{I^+_{Off}}{I^+_{On}}$ is a constant. That ratio has been measured at several He flow rates and is shown in figure 4–8. It shows that this is not a constant value but rather that the fraction gets larger the smaller the He flow. This highlights that the approximation being developed in the present work only holds for very small He flow.

The value that should be used is therefore the limit of the ratio as the He flow goes to 0. The value is extrapolated by fitting the data to a line and extracting the $y-$intercept. The limit in the ratio is therefore $\frac{I^+_{Off}}{I^+_{On}} = 1.105$. The metastable fraction can then be extracted as

$$f^* = \frac{2 - 2 \cdot \frac{I^+_{Off}}{I^+_{On}}}{(\frac{I^+_{Off}}{I^+_{On}} - 2)(A-1)} = 9.78\%. \tag{4.7}$$

Thanks to preferential ionisation, the fraction of the ion beam after the He cell that was in the metastable state as an atom is expected to be higher than for the neutral beam. Naming the ionised beam from the metastable atoms F^* and the remaining part of the beam F, we have, using the same approximation as before for low He flow,

$$\begin{aligned} F &= \sigma\pi f \qquad \text{and} \\ F^* &= A\sigma\pi f^*. \end{aligned} \tag{4.8}$$

The fraction of the ion beam that comes from the metastable atoms is then given by

$$\begin{aligned} \frac{F^*}{F+F^*} &= \frac{Af^*}{f+Af^*} \\ &= \frac{Af^*}{1+(A-1)f^*} \\ &= 26.92\%. \end{aligned}$$

Of course this value is defined only for the limit case of very low He flow; however, it gives a good insight of the fraction of the ion beam to be delivered that can be polarised, giving a polarisation of about 15%.

4.6 ^{20}F polarising transition hyperfine splitting

The quadrupole moment of ^{20}F can be neglected to first order for this study [10]. Equation 2.3 shows that only three factors vary from one isotope to the next, that is μ_I, I and A. Then we can write

$$\frac{I \cdot A}{\mu_I} = \text{constant}, \tag{4.9}$$

from which it can be deduced that

$$A_{20} = \frac{I_{19} \cdot A_{19}}{\mu_{I19}} \cdot \frac{\mu_{I20}}{I_{20}}. \tag{4.10}$$

The spins are known to be $I_{19} = 1/2$ and $I_{20} = 2$ while the moments have been studied previously [10] with $\mu_{I19} = 2.63$ nuclear magnetons and $\mu_{I20} = 2.09$ nuclear magnetons. Altogether this reduces to

$$A_{20} = A_{19} \cdot 0.20. \tag{4.11}$$

The projections are $A_{5/2} = 529.1(1)MHz$ and $A_{7/2} = 313.2(1)MHz$ for ^{20}F. This isotope has a hyperfine structure with $2 \cdot I + 1 = 5$ components for each level, as seen on figure 4–9.

The scheme for polarisation requires exciting all the hyperfine levels of the metastable state, or at least the most populated. The proposed scheme uses an electro-optical modulator (EOM) and an acousto-optical modulator (AOM) to excite all levels except $F = 1/2$. The fundamental laser frequency excites the $F = 7/2$ to $F = 9/2$ transition.

Using an EOM to create laser sidebands, one can excite the transition from $F = 9/2$ to $F = 11/2$ that is $658MHz$ higher than the fundamental.

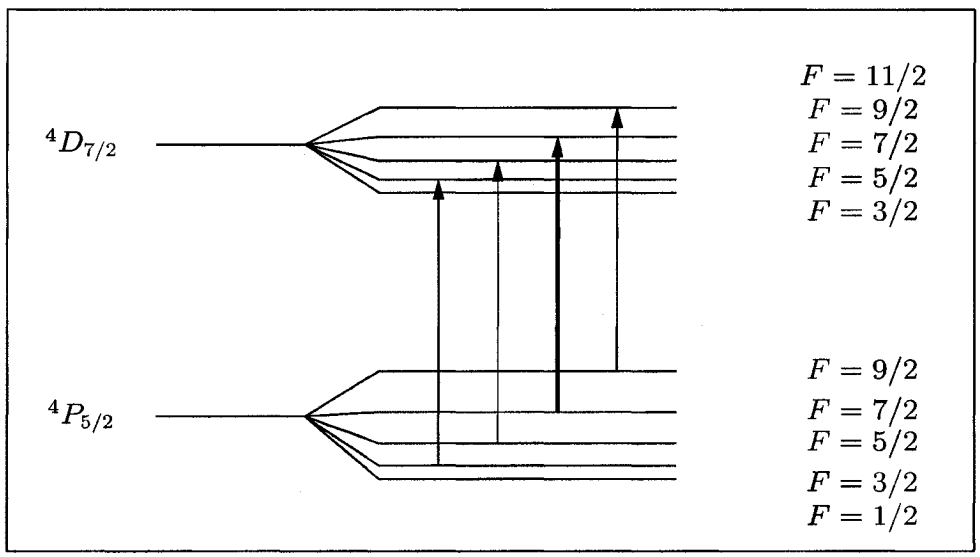

Figure 4–9: Hyperfine structure for the polarising transition in ^{20}F. Note that the diagram is not to scale.

The $F = 3/2$ to $F = 5/2$ transition is $668MHz$ lower than the fundamental frequency. Both those transitions are within reach with a slightly broadened laser and an EOM set at $663MHz$.

The components of the metastable state not considered so far are $F = 1/2$ and $F = 5/2$. The first one has the lowest statistical weight and none of the excited states can decay into it. It is therefore neglected in the current scheme. The $F = 3/2$ to $F = 5/2$ transition is $441MHz$ higher in frequency than the fundamental. It can be reached by double-passing the light through a $111MHz$ AOM as shown in figure 4–10.

The 19 and $28MHz$ EOMs, already used in the present setup, broaden the laser bandwidth. The $663MHz$ EOM provides the $\pm 663MHz$ sidebands. The laser light would then go straight through the beam splitter cube, twice through the quarter wave plate and the $-111MHz$ AOM, producing frequencies shifted down by $222MHz$ and polarisation rotated by $\pi/2$, and finally be reflected by the polarising beam splitter. The final frequencies and their use are summarised in table 4–3

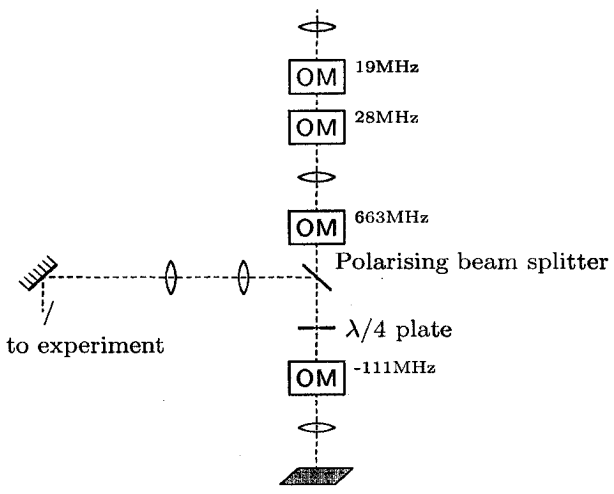

Figure 4–10: Proposed laser setup for polarising ^{20}F.

Table 4–3: Polarisation transition scheme for ^{20}F

Treatment	Frequency shift $[MHz]$	Excited transition F_{lower} tp F_{upper}
Fundamental	0	7/2 to 9/2
EOM	+663	9/2 to 11/2
EOM	−663	3/2 to 5/2
AOM	−222	NONE
EOM + AOM	+441	5/2 to 7/2
EOM + AOM	−885	NONE

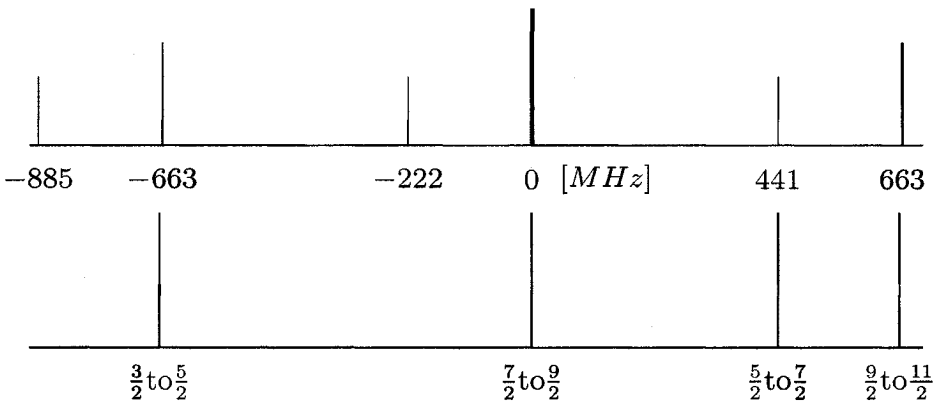

Figure 4–11: Polarisation transition scheme diagram for ^{20}F. The laser beam components are shown in the upper diagram with the tallest line for the laser fundamental frequency, the middle lines for the EOMs sidebands and the smallest lines for the AOM extra components. The transition frequencies are shown in the bottom diagram.

CHAPTER 5
Isotope shift of neutron deficient La isotopes

Mass models predict the binding energy of a nucleus and various parameters that determine the mass of the atom from its different constituents. One output of those models is the mean square charge radius of the nucleus, $\langle r^2 \rangle$, that also gives insight on the deformation of the nucleus. The lanthanides have an increase of the quadrupole deformation and a decrease in triaxiality as the neutron number decreases from $N = 82$ to the mid-shell closure of $N = 66$ [11].

The study of the change in $\langle r^2 \rangle$ of neutron deficient lanthanides at ISAC, starting with the lanthanum isotopes, will confirm those preliminary observations based on decays. The system first needs to be installed and commissioning with the stable isotope ^{139}La is required.

5.1 Atomic structure of lanthanum

Lanthanum is the first of the rare earth elements. Its ground state is therefore in a high shell, $5d^2\ ^3F_2$, as expected for the elements in the middle of the periodic table. The overlap between the nuclear wavefunction and the atomic wavefunction of a d-electron is far less than with an s-electron[1] . This implies that the isotope shift measured starting from a $p-$ or $d-$electron will be only a few percent that of an $s-$state. That is why the present study starts from a metastable state made of two s-electrons, $6s^2\ ^1S_0$.

[1] equation 2.9 for relevance.

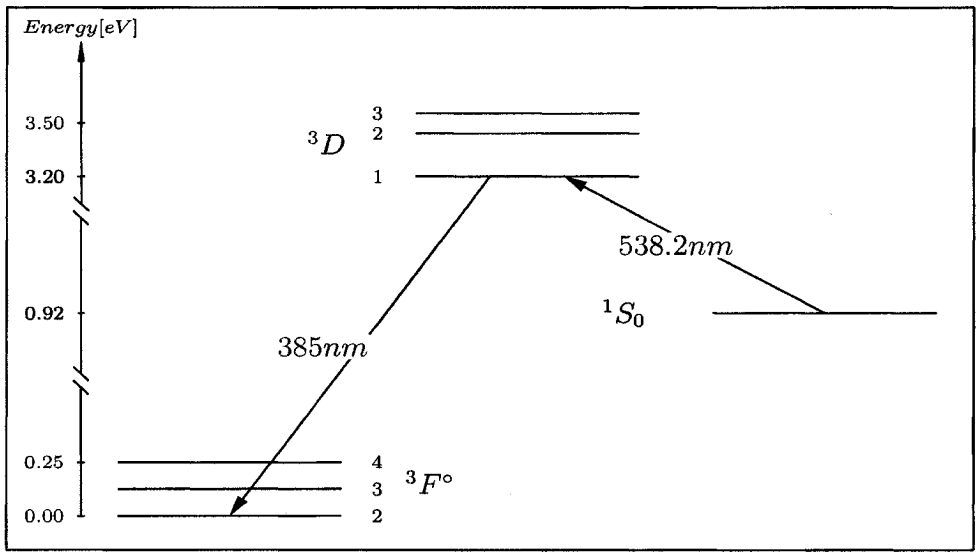

Figure 5–1: Lanthanum ionic structure. Only the levels relevant to the isotope shift study are represented.

The metastable state of the outer electron is produced thermally at the ion source. The Boltzmann distribution predicts that the proportion of metastable ions will be very small for, as shown on figure 5–1, its energy is almost $1eV$ high. Moreover it follows that the higher the temperature, the higher the population and thus the response of the system, but the shorter the source lifetime. There is therefore a compromise to be made between the source lifetime and the metastable population.

The transition of interest is the one from the metastable state to the $5d6p\ ^3D_1^\circ$ state. The main advantage of this transition beyond the $s-$electron is the low angular momenta involved, namely from $J = 0$ to $J = 1$, leading to a hyperfine structure on the excited state with only three components. The other advantage is that the population is not split between sublevels at the metastable level and therefore the whole metastable population is within reach of the laser.

5.2 Ion beam positioning and beam overlap

The system is used in collinear geometry, as described for ions in section 3.3.2 for the equipment and section 3.4.2 for the lasers. The schematic of the setup is recalled on figure 5–2.

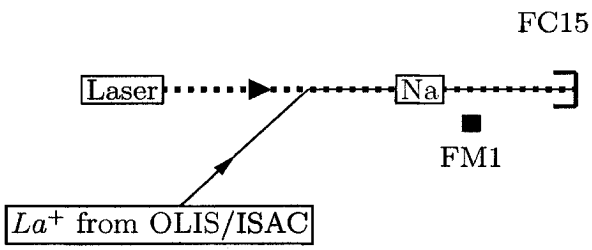

Figure 5–2: Schematic of the Polarizer beam line for the lanthanum study. The solid line represents the lanthanum ion beam while the dashed line represents the laser beam. FC15 refers to the Faraday cup used as a beam dump and FM1 is Fluorescence Monitor 1. Na is the charge exchange cell, included only to indicate its position as it is not used in that system.

Unlike the polarisation setup that has been in place for several years, and therefore has very few alignment issues, the setup for isotope shift study of lanthanides is very recent with different optical and electrostatic components, such as the post-acceleration electrodes, apertures and laser system. The overlap between the laser and ion beams is critical; if those beams miss each other, the interaction cannot occur and the response of the system will be null.

As the lasers are coming from opposite directions from the contra-linear setup and as the apertures are different, the alignment guides from that

system cannot be used and a new method has to be devised. Both the laser and the ion beams can be steered from the outside of the evacuated line. The laser beam is adjusted with the help of the last mirrors prior to entering the vacuum. Unfortunately the 3-meter long lever arm from the mirror makes any adjustment much more sensitive. The ion beam can be steered and focused using deflector plates and electrical quadrupoles in front of the Na charge exchange cell.

The alignment of the ion beam is provided by the plates at the front and back of the post-acceleration region which are segmented into four quadrants. The portion of the beam intercepted by the copper produces a current that is read outside the vacuum; the tuning procedure is to let the ion beam pass through the two front and black plates so as not to hit any of the quadrants, or at least to hit them evenly.

The alignment of the laser beam is done off line prior to taking beam. The beam line is opened up and the coarse adjustment is made by diffusing part of the laser beam to shine on the quadrant and create a shadow, while some of the beam still goes through[2] . It is then possible to visually align the laser beam in the center of that shadow. The fine tuning is done once the system is under vacuum by minimising the background on FM1, for most of that background is due to scattered light from one of the post-acceleration apertures being hit unevenly.

This method can achieve very precise overlap between the two beams and yield results that will be presented in section 5.5. However the overlap is spoiled when the laser beam fluctuates at its source. It follows that the beam wanders and, unlike the ion beam that can be probed continuously

[2] using lens tissue for example.

through the segmented quadrant plates, the laser cannot be probed inside the vacuum. Moreover, the lever arm for adjustment can yield too great a change and then the coarse tuning is lost completely. This is a weakness of the current overlap tuning and improvements are currently underway.

5.3 Sensitivity study

It is important to estimate the sensitivity of the system since this determines the minimum ion beam intensity that is required in a measurement. Three factors have to be considered: the ion beam, the laser beam and the light collection system. These will be discussed in this section and the optimisation work performed on the three of them detailed.

5.3.1 Lanthanum ion beam

The stable lanthanum ions are produced at the OLIS using a microwave ionisation source. This type of source expects to populate the metastable state more favorably than a thermal source.

5.3.2 Laser beam

At low laser power the interaction rate is proportional to the laser intensity. However, if the intensity is increased further the interaction rate will reach a limiting value since the lower and upper levels of the transition approach population equilibrium. That point is called the saturation intensity for the transition.

It is shown in figure 5–3 that the signal keeps increasing almost linearly with the laser power even at $70mW$. The laser power can be increased beyond that value for radioactive run by changing the dye for a fresher lot.

5.3.3 Light collection system

This is the last element of the system that has a direct influence on the sensitivity. Improving the light collection efficiency increases not only

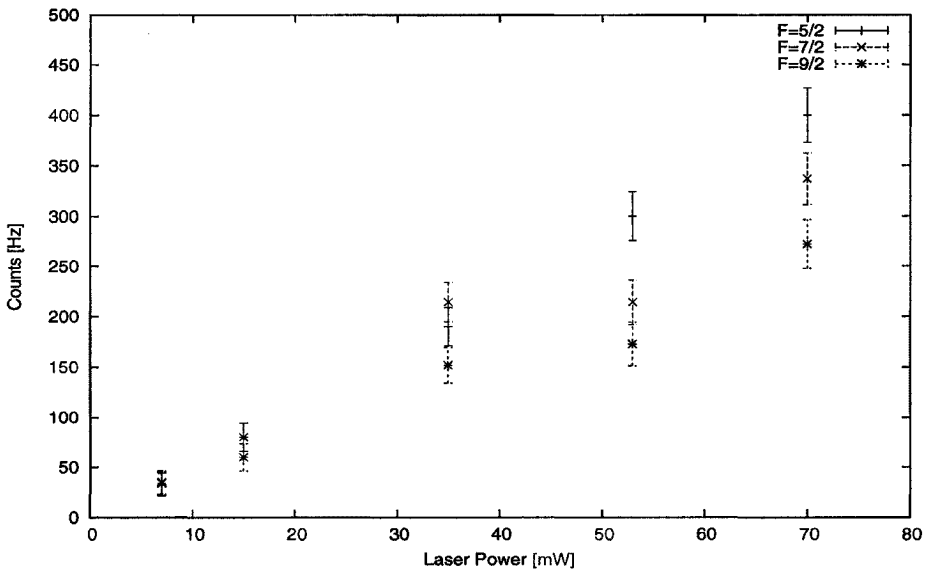

Figure 5–3: Dependence of the peak height of the fluorescence spectrum of the $^1S_0$ to $^3D_1$ transition in the stable ^{139}La with laser power. The three labels refer to the three components of the hyperfine structure of the upper state and will be identified on a spectrum in section 5.5.

the signal, but also the background. Both the collection layout and the background will be discussed in this section.

The background, b, has several origins that can be more or less suppressed and it affects the sensitivity of the experiment directly. The complication introduced by the background is not so much about its size but rather the size of its fluctuations, called the noise, n, of the experiment.

Fluorescence monitoring is a counting experiment and has therefore a Poisson distribution for which the fluctuation is evaluated to be the square root of the number of counts. It follows that the noise on the signal is the square root of the background,

$$n = \sqrt{b}. \tag{5.1}$$

The interest in this experiment is to maximise the ratio of signal-to-noise. The two obvious ways are to increase the signal while decreasing the background, and therefore the noise, to get linear increase in that ratio. It should be noted that increasing the overall efficiency of the experiment increases the signal and the background linearly, therefore increasing the ratio as the square root of the increase. This last component should not be neglected for it could still be the source of great improvement.

Observation region

The transition probing the lanthanum is a depopulating transition, emptying the metastable state as the excited state decays into the ground state of the atomic structure. This is a rapid process and the optical pumping takes place within the entrance of the post-acceleration main stage. This is not a restriction in itself as it does not affect the number of ions observed.

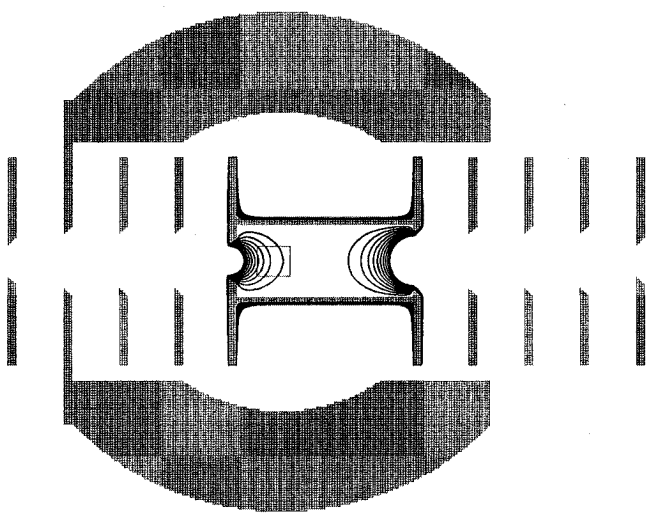

Figure 5–4: Observation region on the post-acceleration electrode. The square in the middle electrode represents the field of view. The dark lines represent the field lines for every 0.1% of the potential from 99% to 99.9% of it.

A great deal of precision is required to ensure that the post-acceleration electrodes are well placed facing the fluorescence monitor whose field of view is a ball of $8mm$ diameter, indicated by a square in figure 5–4. If the observation region is too far upstream, the ions are in resonance in a non-uniform field and the low energy tail can be seen, giving rise to highly asymmetric peaks as shown in figure 5–5. If the observation region is too far downstream, the ions have been optically pumped out and only very few are left to be seen. Altogether the field of view has been placed optimally to get as symmetric peaks as possible with reasonable response.

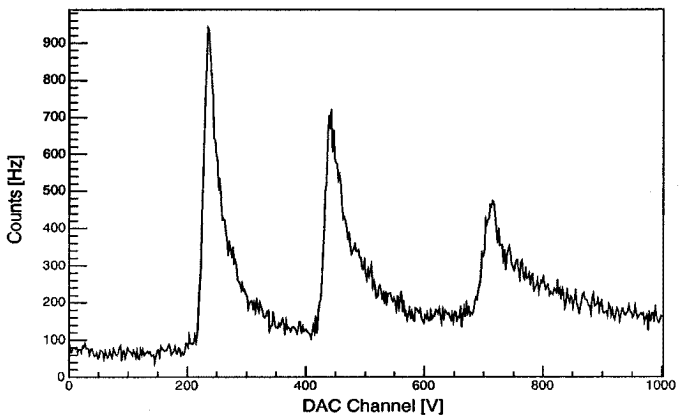

Figure 5–5: Lanthanum spectrum with the post-acceleration shifted to have the observation region too far upstream. The peaks are asymmetric because of the field nonuniformity at the entrance of the main stage of the post-acceleration.

Another limitation of the observation region is its solid angle. Using an $f1$ lens system only allows 9% of the interaction region to be observed. With an added metallic spherical mirror, whose reflectivity is 80%, a factor of 7.2% can be added, for a total light collection solid angle of 16.2%. This limitation is due to geometrical constraints on the beam line and the photomultiplier tube.

Major redesign could probably increase this solid angle using a bi-focal elliptical mirror with one focus at the interaction region and the other at the fluorescence monitor, as originally used at JAERI for the long-lived lanthanum isotopes study [12]. However extra constraints make such light collection setup slightly more complicated, especially because of the diagnostic segmented quadrant plates discussed in section 5.3.1 or the intermediate stages of the post-acceleration electrode. All those issues are currently under further study in order to optimise the system.

In addition to the solid angle restriction, there is the light transfer efficiency to consider. The collected photons in the current system have to go through the mesh electrode, three lenses, three filters, discussed further in this section, and finally trigger the photomultiplier tube of the fluorescence monitor. The efficiencies of those parts are shown in table 5–1.

Table 5–1: Efficiency of the different optical elements in the light collection system.

Optical Element	Efficiency [%]	
Mesh Electrode	80	highest available grade
Lens (×3)	$96^2 = 92$	4% loss per surface
UV Filter	90	maximal value in the range of interest
Glass Filter (×2)	50 to 85	transmission depends on the wavelength average at 70
photomultiplier tube	80 to 60	transmission depends on the wavelength average at 70

Altogether we can get an estimate of the detection efficiency η by combining the solid angle and the transmissions as

$$\begin{aligned} \eta &= (0.09 + 0.80 \cdot 0.09) \cdot 0.80 \cdot (0.96^2)^3 \cdot 0.90 \cdot 0.70^2 \cdot 0.70 \\ \eta &= 0.03. \end{aligned} \tag{5.2}$$

It appears evident that there is much to gain from increasing the efficiency of the experiment. However doing so without compromising the spectrum requires further study.

Background suppression

Reducing the background is a key to reducing the noise in the experiment. The noise has many different sources, as seen from table 5–2.

The base line of the background comes from the photomultiplier tube itself. It has a dark current of $20Hz$. This value depends on the make of the tube but also on the running temperatures. The photomultiplier tube used in this experiment is constantly cooled by a fan. Cryogenic cooling might reduce the background slightly but not considerably.

The vacuum in the beam line is ensured by several turbo pumps along the Polarizer. The pressure is measured before and after the interaction chamber and reaches values as low as $5 \cdot 10^{-7}Torr$. The remaining gas molecules could then be in the path of the ion beam. Collisions between the energetic beam and the rest gas molecules result in fluorescence, called Hühnermann leuchten. The fluorescence this induces is in the UV range of light and therefore a glass filter for those wavelengths is used in the light collection system. The magnitude of the transmitted light is dependent on the vacuum pressure. At the working conditions of the Polarizer, a value of $0.25Hz$ per pA of beam is achieved. A typical ion beam current level from ISAC is $60pA$, leading to a background of $15Hz$.

The laser beam contributes to the background too, in an even bigger proportion than the ion beam. The laser beam itself is focused and should not be seen from the side of the beam line where the fluorescence monitor is set. The beam, however, scatters from some surfaces or some molecules. That scattered light reaches the light collection system and could overwhelm

Table 5–2: Background sources before and after

Background Source	Original System	After Reduction
photomultiplier tube Dark Current	$20Hz$	
Residual Gas Collision	$0.25Hz \cdot pA^{-1}$ of isobaric beam	
Laser Scattered Light	$3.25Hz \cdot mW^{-1}$	$0.33Hz \cdot mW^{-1}$
Activity at FC15	$1.5Hz \cdot pA^{-1}$ of isobaric beam	NONE
TOTAL	$425Hz$	$65Hz$

the fluorescence monitor. The first step towards reducing this contribution to the background is to introduce glass filters. As seen from figure 5–1, the excitation, and therefore the laser frequency, is a yellowish green while the decay from the excited state is blue. As the acquired photons are observed from the decay transition, only the blue is of interest. The use of blue glass filters then provides the best filtering, with a transmission up to 80% for the wavelength of interest and a transmission of only 0.01% in the green. Two of those filters are coupled together for a suppression of the laser background of 8 orders of magnitude. This filtering reduces the contribution to the background at $3.25Hz$ per mW of laser beam, resulting in about $300Hz$ under normal running conditions.

The second step to reducing this value is to look at its origin. One of them is excitation of molecules in the vacuum; that is already minimal for the vacuum is reduced to work against Hühnermann leuchten. The main contribution is actually the scattering from the many surfaces on the beam line. Those surfaces are the plate surfaces, the plate apertures, the mesh electrode and the Faraday cup. All those elements have to be optimised to reduce laser scatter, both geometrically and optically.

Geometrically, the apertures are widened where the plates are not used for diagnostics or measurement, leaving only the diagnostic quandrants and the entrance of the mesh electrode of $8mm$ diameter. The apertures are

also shaped into knife-edges in order to reduce the scattering surface to a minimum. Finally, the inside of the beam dump is machined into a cone and the aperture of the Faraday cup is machined to a knife-edge.

Optically, all the shiny metal surfaces are a source of undesired scatter. To reduce the reflection, the surfaces are sand-blasted to produce a matte surface and blackened. Several options are possible from paint to soot to chemical treatment. Due to handling difficulties, the soot option cannot be used, despite its high light absorption. The plates for the post-acceleration electrodes and the entrance of the Faraday cup are blackened through a process called black oxide [13]. The chamber that everything mounts on is anodised black and finally the inside of the Faraday cup is covered with a graphite paint that does not compromise the vacuum. The only piece that is not blackened is the mesh electrode, for chemical processes would compromise its conducting capability and any paint or soot would deteriorate its transmission. The scattered light background is reduced by an order of magnitude to $0.33Hz$ per mW of laser power, that is about $30Hz$, the same order of magnitude as the other contributions.

The final contribution comes from the Faraday cup dump. As seen on figure 5–2, the Faraday cup FC15 used for dumping the radioactive beam is only $75cm$ from the interaction region. As a consequence, the $\gamma-$rays emitted by the decaying elements accumulated at that point are energetic enough to pass through the aluminum beam line and trigger the fluorescence monitor by interacting with the photocathode. For an unshielded source, the observed increase in background is $1.5Hz$ per pA of isobaric beam, that is $90Hz$ of background. After adding a graphite coated lead pipe in front of the Faraday cup, bringing up $5cm$ of lead in the line of sight of the photomultiplier tube, this source of background disappears completely.

This reduction in the background resulted in the reduction of the noise from $21\sqrt{Hz}$ to $8\sqrt{Hz}$, improving the signal-to-noise ratio by a factor of 3.

Statistical enhancement

The estimate of the noise for the radioactive run is of $8\sqrt{Hz}$ for which the ion beam is considered to be $60pA$, with only $1pA$ of lanthanum. The response from the test runs with stable lanthanum, discussed in section 5.5, showed a response at the level of $4Hz$ per pA. Even though the source types and the metastable populations are different, this should still be a good estimate of the system sensitivity. The expected signal-to-noise ratio over $1s$ is therefore $1:2$, which means that any signal would be buried in the noise.

To identify a peak a signal-to-noise of $2:1$ is required. The way to achieve such improvement without changing the system any further is to increase the statistics. As more time is spent on each channel, the signal and the background both raise linearly. However, the noise goes as the square root of the background, as shown in equation 5.1, and thus the ratio of signal-to-noise goes as $time:\sqrt{time}$, which is the square root of the time. Therefore, in order to gain a factor of 4 on the signal-to-noise ratio, there must be an increase to $4^2 = 16s$ per channel.

This permits an estimate of the time required to acquire a spectrum. Assuming that a 500-channel scan permits peak identification, this makes $16 \cdot 500 = 5300s = 1h30min$, for negligible dead time and a run with radioactive beam for the largest peak.

It is important to note that the radioactive lanthanum ions are produced at the ISAC surface ionisation source from which we expect only 1% population[3] or less in the metastable state than in the ground state.

[3] $1eV$ level at $2500K$.

That is a definite reduction of the sensitivity for any study from the ground state would be higher by two orders of magnitude. However, the field shift contribution to the isotope shift from the ground state would be too small, as mentioned in section 5.1.

5.4 System stability

Statistical averaging can provide the improvement of signal-to-noise required for the experiment to be feasible. However, any fluctuations in the system would considerably compromise this enhancement. If any parameter of the system wanders from its set value, the acquired data could not be added to previous spectra for averaging. It is therefore required that the system be stable for long periods of time, for the ion beam as well as for the laser beam.

5.4.1 Ion beam stability

The ion beam has two main properties that could compromise averaging. The first is its energy and the second is its intensity. The beam energy is controlled through three power supplies, as discussed throughout section 3.3, one at the source and two at the post-acceleration electrodes.

The source power supply and the Harrison power supply are both set to a given value and are only required to maintain it; it has been discussed already in previous sections that despite the low precision on its readback, the stability and reproducibility of the source supply is high and will therefore not be a concern for this experiment.

The Harrison supply has been studied and as it is not in a temperature-controlled environment, it is subject to fluctuations over a full day as the room temperature varies. The extent of those fluctuations is $\pm 0.5V$ over several days. It is therefore not a concern as long as the channel width is bigger than this, for acquisition over several day periods.

Finally, the Kepco power supply is the one being scanned. The precision on the DAC is greater than the Harrison stability and the scanning Kepco power supply, operating as an amplifier, only transmits its input. The linearity of the output is very reproducible and accurate. In order to insure that as few parameters as possible are left unknown, the combined potential applied on the post-acceleration electrodes is monitored at each channel and recorded with the data with an precision of $\pm 0.1V$. Hence, for as long as the channel width is kept within $0.5V$ the ion beam energy is stable for several hours.

The other ion beam parameter that affects the statistical averaging is the beam current. If this fluctuates over different channels, the background as well as the signal are affected. It is true that the greater the ion beam intensity, the better the signal-to-noise ratio. However, a burst of beam in the middle of a scan would compromise its statistical value. That is why the channels are scanned relatively quickly, with an acquisition time of only $1s$ per channel, so that the scan of the full range only takes $500s$. The repetition of those scans averages out over the long time beam intensity fluctuations. As a monitor of this parameter, the current at the Faraday cup dump is recorded continuously with the data, similarly to the post-acceleration potential.

5.4.2 Laser stability

The laser beam has two properties, that could compromise statistical averaging, its frequency and its intensity. The first is dependent on the dye laser adjustments while the latter could be influenced by both the dye and the argon ion lasers.

The laser frequency is set by several optical elements in the dye laser, all susceptible to mechanical fluctuations due to environmental changes.

The most important environmental factor is the temperature of the room. The air in the laser hut in which the lasers are working is not temperature-controlled and therefore its temperature suffers from day-night fluctuations as well as heating up as the lasers release heat into the room. If left drifting freely, although locked to an internal cavity, the dye laser frequency is specified by the manufacturer to wander at a rate of $250MHz$ per hour. It is important to note here that these fluctuations are not continuous but rather occur as bursts and sudden changes. This is tolerable for acquisition of stable spectra where the overall process takes 15 minutes.

These conditions are definitely not useable for a radioactive run, where the minimum acquisition time has been estimated to be 90 minutes. A frequency lock therefore needs to be implemented in the system. An iodine cell provides a reference from which the laser beam frequency is evaluated and a correction signal is issued into a feedback loop to the dye laser. The first version of this frequency lock, as described in appendix C, provides a frequency stabilisation to $50MHz$.

Considering the running conditions for a radioactive beam[4] and the appropriate frequency, the scanning can be evaluated to be $6.5MHz$ per V. It follows that a $50MHz$ uncertainty corresponds to a $7.5V$ width. There is therefore no point in having the channels smaller than $5V$. The advantage of that is the reduction of the number of channels over the $1kV$ range, and therefore of the acquisition time.

The other parameter that can affect the statistical averaging is the laser power. As the laser power drops, or rises, the background fluctuates as well as the signal. Although the signal increases with laser power, if there is a

[4] mass $131amu$, $E = 30600eV$

sudden burst in the power in the course of a scan, the overall scan is lost for the statistical averaging. The laser power is therefore monitored and recorded in the data acquisition.

Note that on top of any fluctuations that could come from thermal expansions in the cavity, there are many factors that can result in laser power change. First the argon ion laser can lose power due to thermal expansion of its cavity; this happens frequently. Another source of laser power drop is the aging of the dye. The lifetime of the Rhodamine 110 used for the lanthanum study is several days, with a pump power of $6W$. It can therefore last over a full acquisition run but requires to be changed when the laser power drops significantly.

5.5 Commissioning

The experiment is the study of spectra of lanthanum with a radioactive beam. The commissioning therefore has to go in two steps, first the observation of a spectrum with any lanthanum beam and then the observation of such spectrum with a radioactive beam.

5.5.1 Stable ^{139}La study

The stable lanthanum ions are produced at the microwave OLIS using solid lanthanum as the source and accelerated to an energy of $14800 \pm 100eV$, as calibrated in the first stage of the analysis. The ion beam has an intensity of several hundreds of pA.

The spectra, shown in figure 5–6, are recorded with a freely drifting laser of $75mW$ power and $18587.49 \pm 0.03cm^{-1}$ frequency. Although no reference lock is used for this study, the drift was not significant over the acquisition time. The spectra provide information on the response of the system and serve as a basis for running radioactive nuclei. It can also be used to extract the hyperfine structure information.

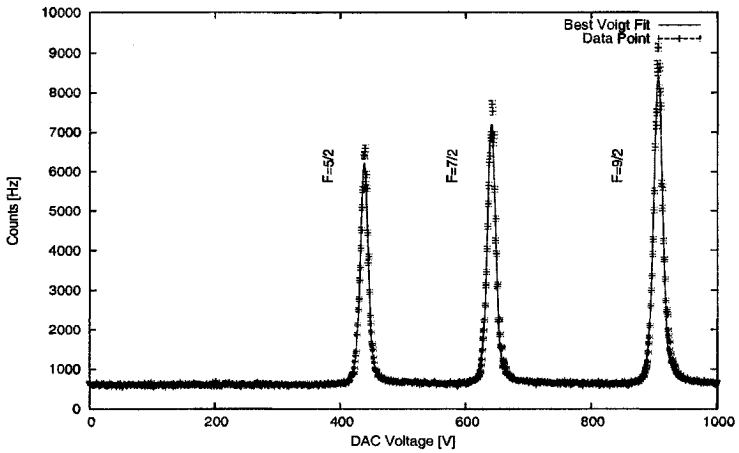

Figure 5–6: Stable lanthanum fluorescence spectrum, single scan

The study of the hyperfine structure was carried similarly as for the fluorine, as described in section 4.4.1. The width of the Voigt profile is split between the Gaussian and the Lorentzian contribution quite evenly with respectively $6.5V$ and $5V$; altogether the width of the peaks is about $100MHz$. The hyperfine constants for the upper state are extracted and the results are shown in table 5–3 together with the measured values from JAERI [12]. The A coefficients agree within the uncertainties. However, the B coefficients are quite different. This matter is being further investigated to understand the origin of the discrepancy.

Table 5–3: Hyperfine constants for the stable ^{139}La $^3D_1$ state.

Coefficient	Measured Value $[MHz]$	JAERI Value $[MHz]$
A	$547.5 \pm 2 \pm 2$	549.1 ± 7
B	$6.2 \pm 2 \pm 2$	26 ± 3

5.5.2 Radioactive ^{131}La study

The radioactive lanthanum ions are produced at the surface source of ISAC and accelerated to an energy set at $30600eV$. The beam produced is

much weaker than the stable beam with a lanthanum fraction up to $1pA$. The study therefore requires the highest level of stability and the optimal running conditions as discussed in the previous sections of this chapter.

The laser frequency was adapted to the different beam energy and used at a frequency of $18591.82cm^{-1}$ with $150mW$ power. The frequency was locked to an iodine reference, as described in appendix C, with a width of $50MHz$. A spectrum was observed, shown in figure 5–7. The assignment of the F angular momenta is tentative at present as the analysis of the spectra is still continuing. However some information can be extracted from preliminary results.

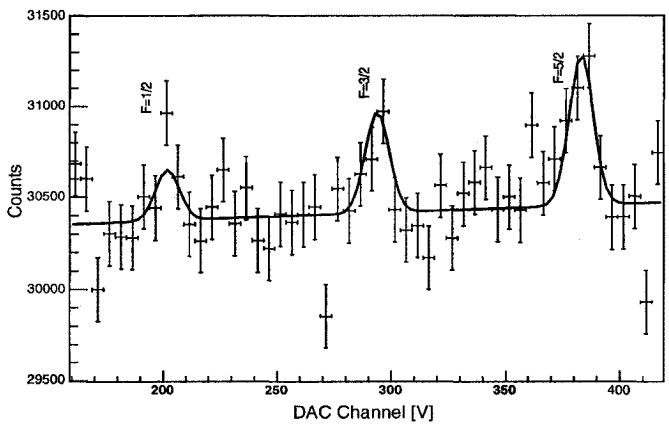

Figure 5–7: Radioactive lanthanum fluorescence spectrum accumulated over 670 scans. The tentative affectation of upper state F values are written on the spectrum.

The acquisition of this spectrum required 670 consecutive scans with $1s$ acquisition per channel for a total of about eleven hours to achieve a signal-to-noise of 2 : 1 through statistical enhancement. This acquisition time is an order of magnitude longer than the estimated time from section 5.3.3, showing that some parameters of the experiment remain unkown.

First of all the metastable population from the ISAC surface source is not known. Since the microwave OLIS operates non-thermally, the two cannot be expected to behave equivalently. The limit in the metastable population is the running temperature of the source that cannot be raised above 2200°C. The alternative to that limit is to wait for other types of ion sources that would provide a higher metastable population or devising a way to actively populate the metastable level.

It should also be noted that the overlap between the laser and ion beams cannot be monitored directly during radioactive beam running. Since there is not a strong enough signal to maximise the response by direct observation, it could be that the two beams are only partially overlaped, which would greatly reduce the signal. Having diagnostic elements with known relative alignment would solve that question for further runs.

The final note on that spectrum is the background. At first glance it would seem that the noise is greater than the statistical fluctuations from a counting experiment. It turns out, as shown on figure 5–8, that the beam current and the laser power did not average out over the 670 scans but rather show a trend both in the same direction. Using a tilted background in the fluorescence spectrum provides then a much better fit to the data and the noise about that baseline is of expected size.

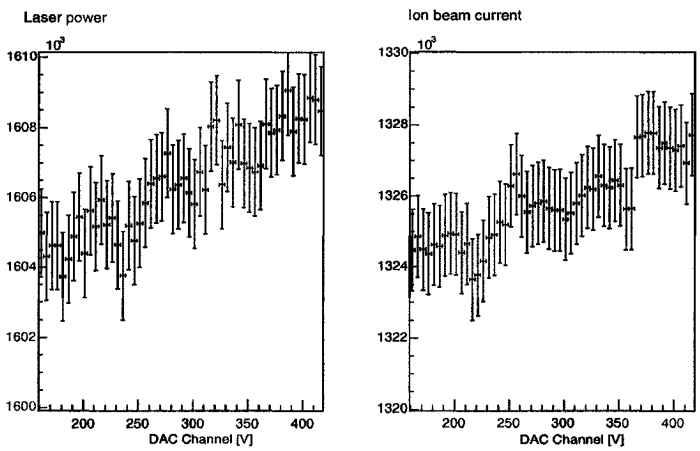

Figure 5–8: Faraday cup and laser power averaged readings over the 670 scans of acquisition for the radioactive lanthanum spectrum. Both graphs show a positive slope to their mean.

CHAPTER 6
Conclusion

Collinear fast-beam laser spectroscopy is a new field at ISAC, with many ongoing developments and upcoming experiments. The polarisation of fluorine seems at hand with a polarisation scheme now designed and a spectrum has been observed with radioactive lanthanum ions.

It has become obvious with those two experiments that many steps remain for improvements in experimental conditions. ISAC cannot yet produce a radioactive fluorine beam for no source has the capacity to ionise it from the target. The new FEBIAD and ECR sources, currently in test and design stages respectively, will breach this gap and permit further study of fluorine, the next step being to reproduce the work performed on the stable isotope with the radioactive isotope in order to ensure that the lines are properly excited according to the scheme.

Another improvement that could be made to the fluorine polarisation is the fraction of the reionised beam that can be polarised. The current scheme relies on preferential ionisation in the He cell where the ground state is still ionised. An alternative to this effect would be to laser ionise the neutral atoms once the polarisation has occurred using a fast pulsed laser beam that would resonantly ionise the metastable atoms alone, therefore making the resulting ion beam completely originating from the polarisable atoms. Such a technique could yield up to 75% polarisation.

The study of the isotope shift in lanthanum is, on the other hand, mostly limited by the sensitivity of the equipment and the use of the metastable level.

Despite all the recent improvements to the setup, the acquisition of the radioactive ion spectrum did not meet the experimenters' expectations. All the improvements performed on the setup focused on potential precision and noise reduction, leaving the signal itself untouched; the next phase of the work will therefore be to try and increase the photon collection to increase the signal strength, as well as improving the monitoring of the laser and ion beam overlap to ensure maximal interaction in front of the fluorescence monitor.

The metastable population from the ISAC surface source is a definite limiting factor. As the source cannot produce any more ions in that state and no other state is of physical interest, the only step to take is to produce the metastable state after the lanthanum has been ionised. The lanthanum ions can be trapped in the TITAN Radio-Frequency Quadrupole (RFQ) and then exposed to laser pulses at $218nm$[1] that excites the ground state to an excited state that can decay to the metastable level of interest. However, the RFQ is still under development and further study is required to develop this method. A different ion source, like the FEBIAD, could provide a higher population as well.

A consequence of using the RFQ to populate the metastable level is the bunching of the ion beam. This method would allow the reduction of background and therefore noise, hereby increasing the signal-to-noise.

TRIUMF's interest in collinear fast-beam laser spectroscopy is expanding beyond those two experiments and what was originally a polarisation line for lithium is now becoming an all-purpose spectroscopy line.

[1] This wavelength could be obtained by quadrupling the TRILIS titanium dopped sapphire laser at $872nm$ or by tripling a pulsed dye laser at $654nm$.

APPENDIX A
Voigt profile

A Voigt profile distribution is the convolution of a Gaussian distribution, given by

$$g(x) = e^{-\frac{x^2}{\sigma^2}}, \tag{A.1}$$

and of a Lorentzian distribution, given by

$$l(x) = \frac{1}{x^2 + \frac{\Gamma^2}{4}}, \tag{A.2}$$

where σ and Γ are the widths of the respective distributions. The Voigt profile is then described as

$$V(x) = \int_{-\infty}^{\infty} \frac{e^{-\frac{y^2}{\sigma^2}}}{(x-y)^2 + \frac{\Gamma^2}{4}} \cdot \mathrm{d}y. \tag{A.3}$$

This profile is defined symmetrically around $x = 0$. This is generally physically not the case and one has to shift the x-axis to the centroid $\bar{x}$ of the peak. The Voigt profile then becomes

$$V(x) = \int_{-\infty}^{\infty} \frac{e^{-\frac{y^2}{\sigma^2}}}{(x-\bar{x}-y)^2 + \frac{\Gamma^2}{4}} \cdot \mathrm{d}y. \tag{A.4}$$

The final step to having a usable distribution for physical use is the normalisation. As it stands, this distribution does not, in a general case, give a total area of probability 1. Introducing the normalising factor N we have

$$V(x) = N \cdot \int_{-\infty}^{\infty} \frac{e^{-\frac{y^2}{\sigma^2}}}{(x-\bar{x}-y)^2 + \frac{\Gamma^2}{4}} \cdot \mathrm{d}y. \tag{A.5}$$

It is now left to evaluate N so has to have $\int_{-\infty}^{\infty} f(x)\mathrm{d}x = 1$ using appropriate integral operations and Lorentzian and Gaussian normalisations.

$$\begin{aligned}
1 &= \int_{-\infty}^{\infty} N \int_{-\infty}^{\infty} \frac{e^{-\frac{y^2}{\sigma^2}}}{(x-\bar{x}-y)^2+\frac{\Gamma^2}{4}} \cdot \mathrm{d}y \cdot \mathrm{d}x \\
1 &= N \int_{-\infty}^{\infty} \int_{-\infty}^{\infty} \frac{e^{-\frac{y^2}{\sigma^2}}}{(x-\bar{x}-y)^2+\frac{\Gamma^2}{4}} \cdot \mathrm{d}x \cdot \mathrm{d}y \\
\frac{1}{N} &= \int_{-\infty}^{\infty} \frac{2\pi}{\Gamma} \cdot e^{-\frac{y^2}{\sigma^2}} \mathrm{d}y \\
\frac{1}{N} &= \frac{2\pi}{\Gamma} \cdot \sqrt{\pi}\sigma \\
N &= \frac{\Gamma}{2\sigma\pi^{\frac{3}{2}}}
\end{aligned} \tag{A.6}$$

Reuniting equations A.5 and A.6, the final Voigt profile, as used in the present work, is

$$V(x) = \frac{\Gamma}{2\sigma\pi^{\frac{3}{2}}} \cdot \int_{-\infty}^{\infty} \frac{e^{-\frac{y^2}{\sigma^2}}}{(x-\bar{x}-y)^2+\frac{\Gamma^2}{4}} \cdot \mathrm{d}y. \tag{A.7}$$

APPENDIX B

Effect of energy uncertainty on hyperfine component measurements

In order to evaluate the effect of the beam energy uncertainty on hyperfine splittings in a general way, a simple, yet non-physical, case can prove to be informative. A good example would be to have some data where two peaks are separated by $500V$, say at $200V$ and $700V$, with same height. Setting the conditions as in the different runs, as summarised in table B–1, the influence of the beam energy uncertainty on the splitting can be extracted.

The splitting is evaluated in MHz by first bringing the peak into frequency space and then comparing the two. This is obtained by using the Doppler shift equation as in equation 3.1. By calculating the splitting at the different values, one can observe the impact of energy uncertainty over a splitting. The extreme values obtained from these calculations are tabulated in table B–2 while the distribution can be seen for the fluorine case in figure B–1. However the final hyperfine coefficient is then calculated from those splittings using the coefficients introduced in chapter 2; the final error on the splitting could then be increased or decreased to span an order of magnitude. Stating that the uncertainty in the splitting then ranges from $5MHz$ to $50MHz$ is conservative. Note also that this uncertainty would be influenced by the splitting itself; the larger it gets, the more it will be influenced.

Table B–1: Experimental parameters used for fluorine and lanthanum

Element	Fluorine-I	Lanthanum-II
Mass $[amu]$	18.9984032(1)	138.9057996(35)
Laser $[MHz]$	436212900(100)	557233800(900)
Energy Set Point [eV]	40806(400)	14256(150)
Lasers	Polarising	Spectroscopy

Table B–2: Influence of beam energy uncertainty on a splitting

	Energy $-\Delta E$	Energy	Energy $+\Delta E$	Δ
Fluorine	$5813MHz$	$5783MHz$	$5755MHz$	$30MHz$
Lanthanum	$4686MHz$	$4660MHz$	$4635MHz$	$25MHz$

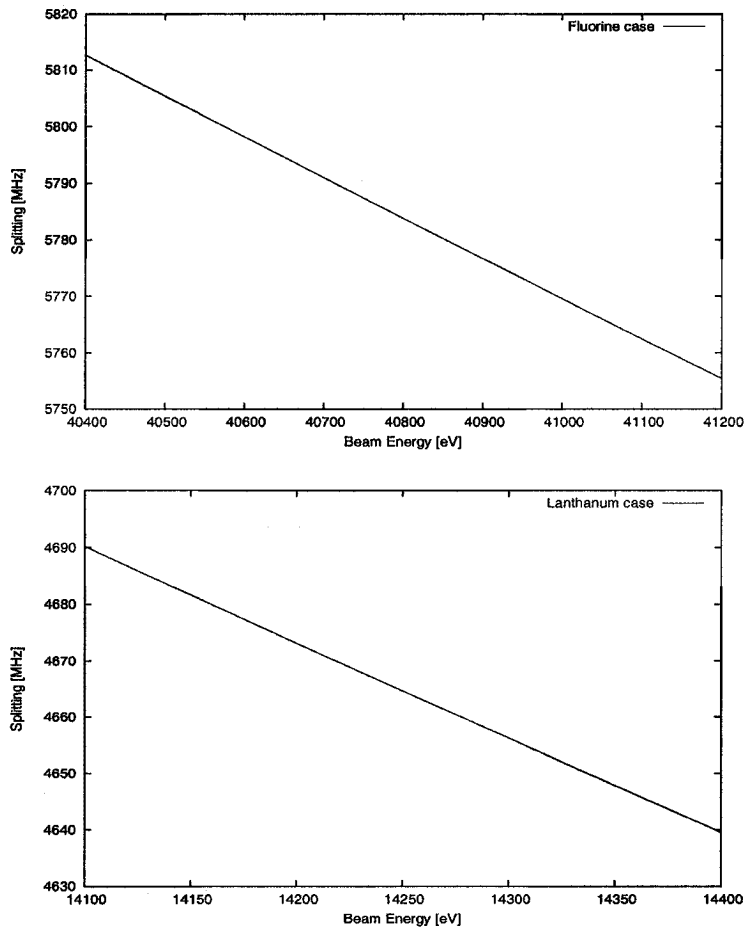

Figure B–1: Splittings for a $500V$ separation in the fluorine and lanthanum running conditions over the range of beam energy uncertainty.

APPENDIX C
Laser locking development

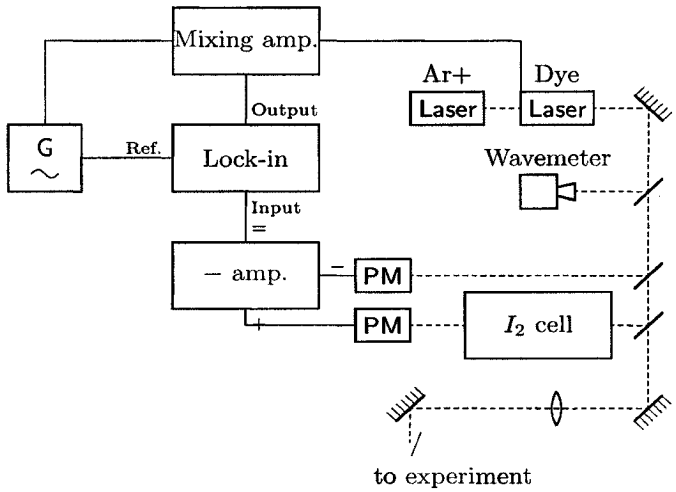

Figure C–1: Spectroscopy laser setup with frequency lock as used for the radioactive run on ^{131}La.

It has been discussed in section 5.4.2 that the laser system has to be stable over long periods of time to allow for statistical enhancement. The manufacturer specifications for the dye laser that provides the final frequency of the laser beam predicts a drift of $250MHz$ per hour which is definitely not acceptable.

With the use of a proper reference there are means to ensure that the laser frequency is kept within reasonable range. In the case of the polarising lasers, as mentioned in section 3.4.1, that reference is provided by a $He-Ne$ laser and a spectrum analyser that is used to compare that stabilised known frequency to the dye laser output.

In the case of the spectroscopy lasers a different approach is considered and the reference is provided by an absorption line in the spectrum of molecular iodine, I_2[14]. The setup is shown in figure C–1.

A waveform generator provides an oscillating signal to dither the frequency of the dye laser by $50MHz$. This dither is performed at a rate of $100Hz$ and is used to scan across the tip of the absorption line. A portion of the laser beam is then picked up at two places with equivalent power by beam splitters using the 4% reflection from the surface of a microscope plate. The first beam is used as a reference while the second is sent through the iodine cell. The power of each beam is read by a photodiode and then the two signals are processed through a difference amplifier, to normalise over power fluctuations. That signal should look as shown on the top graph of figure C–2 if the whole absorption line were scanned; however, the $50MHz$ dither should only span its tip.

The absorption line signal is then sent through a lock-in amplifier in order to differentiate it and extract the component from the frequency dither. The output of the lock-in amplifier translates the top graph into the bottom graph of figure C–2. That correction signal is then mixed into the dither signal and fed to the dye laser to correct for any change in the laser frequency.

The feedback is taken directly from the derivative signal. If the laser frequency wanders from the centre of the absorption line, the derivative deviates from 0. If the frequency rises, so does the derivative and if the frequency lowers, the derivative goes negative. The problem is that then the laser would be pulled even further from the peak and the lock would be lost instantaneously. The solution is to reverse the phase of the lock-in amplifier and output the opposite signal from the one pictured in figure C–2. The

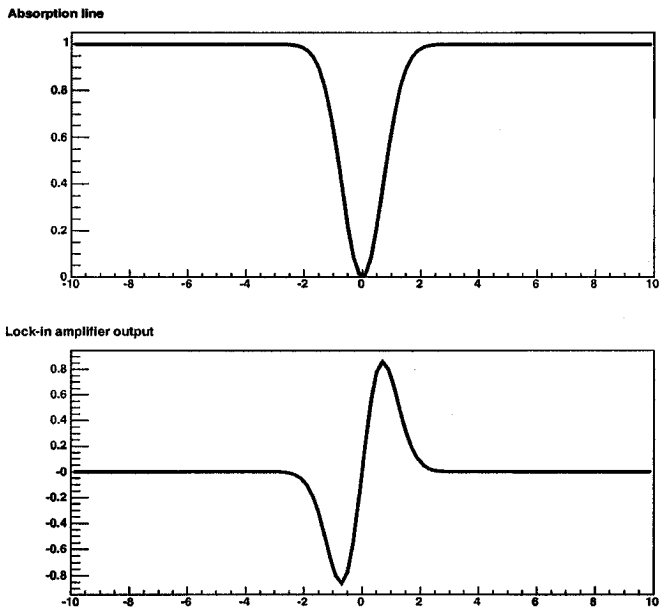

Figure C–2: Laser lock signals. The top graph represents a typical Gaussian absorption peak. The bottom graph represents its derivative as processed through a lock-in amplifier.

laser frequency will then be pulled back toward the center of the line as it starts to drift.

The system only allows for specific frequencies to be used as the laser has to be at a frequency from the iodine spectrum. That spectrum has a wide range of transitions and it is generally quite easy to find one that is appropriate, provided that the Doppler tuning can be adjusted, using the Harrison power supply.

While running with radioactive lanthanum, this system maintained the laser frequency very stably over several hours with only a $50MHz$ extra width for the dither. This allowed for the long acquisition of the spectrum 5–7. The loss in laser beam was then deemed more to the Ar^+ laser power loss.

The next stage of laser lock development is to reduce the dither to be able to use a narrower laser line. Ultimately, the use of a Doppler-free lock where the thermal distribution of the iodine molecules in the cell can be overcome would achieve a lock with barely any dither on the laser frequency, therefore making the experiment unaffected by the laser lock.

APPENDIX D
Acquisition system overview

The data acquisition for the experiment is a non-negligible element, even though it never appears directly in the conceptual discussion nor on the setup description. The first and properly most important note on the data acquisition system, PolDAQ, is that it does not only record and store the data, it also drives the experiments, therefore providing a completely integrated system for the experiment.

D.1 Software

D.1.1 MIDAS

PolDAQ is one of the many systems using the Maximum Integrated Data Acquisition System (MIDAS) at TRIUMF. Each voltage step from the DAC is treated by MIDAS as an event. At each event, MIDAS performs a series of tasks: incrementing the voltage to the next step and sending the information to the DAC, waiting for the power supplies to stabilise, clearing the scalers and ordering the digital voltmeter to read the potential[1] , waiting for the acquisition time and finally retrieving and logging all the measurements from the digital voltmeter and the scalers.

It becomes evident that a single program cannot perform all the tasks at once and it is therefore segmented to allow for greater performance. Moreover, extra software components watching over the acquisition process extend the power of the acquisition system for more versatility.

[1] as mentioned in section 5.4 about potential stability.

D.1.2 Main front end

This program is the core of the acquisition and drives almost all the others. This program takes the information given by the experimenter and calculates the real parameters to be given to the other pieces of software and to the hardware in the appropriate language. It initialises the acquisition and starts the program.

This program calls all the commands at each step for any task to be performed, from voltage increment to scaler reading. The timing is made through a programmable pulse generator (PPG) that will be discussed with the hardware in section D.2.3. It also creates the banks used for transferring the data to the logger, discussed in section D.1.4. Before sending any bank to memory, it verifies that some parameters are within thresholds defined by the experimenters; if the laser power or the ion beam current changes from its original value by more than an allowed threshold, the acquisition will be paused until the parameters are back within acceptable limits.

D.1.3 DVM front end

The digital voltmeter needs to be driven on its own by a different front-end for it requires very specific commands to perform its task. Moreover, unlike the other components which communicates over the intranet, the digital voltmeter communicates via GPIB, a protocol for which cable length has to be kept to a minimum.

The DVM front end issues the appropriate commands when ordered by the main front end in order to increment the DAC voltage to be fed to the Kepco power supply or to read the potential from the digital voltmeter.

D.1.4 Logger

The purpose of the logger is to log the data while it is being acquired. At each event there are several setting parameters to be saved as well as the scalers and the digital voltmeter readings.

The logger works by retrieving the banks produced by the main front end. In the case of PolDAQ, two banks are being used, named CYCI and HSCL. The first records the running parameters together with the DVM readings while the latter is for the scalers. All those are dumped into a single data file per run that is updated at each event, a property that is important for monitoring the experiment on the fly as shall be discussed in section D.1.5.

D.1.5 Analyzer

While acquiring the data, it is important to be able to see the evolution of the parameters as well as the acquired spectra. Moreover, some hardware parameters such as the laser power of the beam current are not controlled by PolDAQ and might need attention. It is therefore needed to witness the experiment as it accumulates.

The analyzer reads the data from the file created by the logger and then creates histograms and graphs from those in connection with an analysis package. In the case of spectrum analysis, ROOT is used to created and display the histograms from the analyzer.

The analyzer can perform some modifications to the data to make them more accessible or issue outputs to satisfy any analysis method, from ASCII files to ROOT histograms.

D.1.6 Lazy Logger

The Lazy Logger is a program that creates a back-up of the data to ensure that any mistake that might be made on the acquired data at analysis can be recovered and that the information is never lost.

D.1.7 Run logger

The run logger is a program that does not interact nor participate to the acquisition. Its function is simply to watch over the acquisition and make sure that all the components are responding and performing their tasks. In the event that a front end dies or that some piece of software gets disconnected from the system, the run logger issues an alarm and stops the run, making sure that the experimenters is aware of any trouble.

D.1.8 MIDAS hypertext transfer protocol daemon

The mhttpD is a program that enables control of the acquisition system over the internet. The acquisition system can then be accessed from any computer with an internet connection. The commands that can be performed then through any internet browser are the setting of the acquisition parameters, the modification of hardware running specifications, the interaction between the programs.

The web interface is also used to start and stop a run and any parameter can be monitored any time on some of its page. It allows international groups to stay connected and participate to experiments without leaving their home institution.

The web interface also issues warning and alarms as triggered by the run logger and all the important messages from all the pieces of PolDAQ are shown there.

Finally the e-log allows for the collaboration to comment on the run as it goes about anything, from the weather to a Nobel winning breakthrough,

from the data acquisition to the hardware issues. That features keeps a collaboration connected beyond the reach of a traditional log-book.

It is important to note that in order to prevent unwanted interaction, PolDAQ web interface is read-only unless the user possesses an access code, delivered by the TRIUMF DAQ Group[2]

D.2 Hardware

D.2.1 Digital voltmeter

The Agilent 34970A digital voltmeter, has two functions. A first digital-to-analog converter (DAC) issues voltages between $-12V$ and $+12V$, a channel of which is used to control the Kepco scanning power supply, by sending a signal up to $\pm 10V$.

The second module is an analog-to-digital converter (ADC) and is used to read the potential from the voltage divider unit placed at the output of the power supplies. With its 18 bits of reading capability, it achieves a precision of $0.08mV$ on the reading that translates into $\pm 0.08V$ on the potential applied on the post-acceleration electrode.

The limits of that piece of hardware come from its local nature that does not make it easy to integrate with PolDAQ, which uses intranet communication. This is why the DVM front end is required. Moreover the measurements on the ADC are made in series, rather than in parallel, and therefore each additional measurement requires more time. Altogether, a single measurement requires $150ms$ between the time the command is issued from the front end and the time the value is returned. This is an acceptable time for a spectroscopy experiment since the scalers are acquiring data for

[2] The contact preson is Renée Poutissou, renee@triumf.ca

a length of time in this range. However, no other ADC can be added to the system for it would start to slow down the acquisition considerably.

D.2.2 Scalers

The scalers acquire counts from any source. They are located in a VME crate at proximity to the experiments.

The main scaler is the one reading the photomultiplier counts, hereby recording the spectra. In the case of particle detection, the scaler records the output of a voltage-to-frequency converter (VFC), taking its input from the lock-in amplifier. The frequency issued, proportional to the voltage input, is measured by the scaler. This method yields good spectra as can be seen in figure 4–6.

In the case of the lanthanum spectroscopy, several extra parameters needed to be monitored in order to ensure that the statistical enhancement was being performed efficiently. Those parameters were the proton beam current for radioactive beam production, the Faraday cup reading at the beam dump for ion beam intensity, the laser power at some pick off for laser power stability and also the output of the laser lock to ensure that the frequency was stable. The proton beam is given as a direct signal to the scaler while the three other parameters are processed through the VFC.

D.2.3 Programmable pulse generator

The PPG issues a very precise timing to the acquisition system. The PPG has ns range capabilities. However, PolDAQ only requires ms delays, from $10ms$ for the power supplies to $1000ms$ for the scaler acquisition. Those timings are therefore very precise.

The connection between the PPG and the front end is assured by a separate program, rf_config that translates the front end intentions into proper code for the PPG. Because of the nature of the PPG, that specific

piece of software has to be initialised prior to the acquisition be started, to interpret properly the acquisition parameters.

D.2.4 Computers

Each front end is run from a different computer. Those are required to operate the pieces of software and also to log the data.

References

[1] C. Schwartz. Theory of hyperfine structure. *Phys. Rev.*, 97:380–395, 1955.

[2] W. Noertershaeuser et al. Isotope shifts and hyperfine structure in the $3d^2d_j \rightarrow 4p^2p_j$ transitions in calcium II. *The European Phys. Journal*, D2:33–39, 1998.

[3] W.H. King. *Isotope Shifts in Atomic Spectra.* Plenum, 1984.

[4] W. Pauli. *Die Naturwissenschaften*, 12:741, 1924.

[5] T. Maiman. Stimulated optical radiation in ruby masers. *Nature*, 187:493–494, 1960.

[6] P. Jacquinot. *High resolution laser spectroscopy*, volume 13 of *Topics in applied physics.* Springer-Verlag, Berlin, shimoda k. edition, 1976.

[7] JL. Cooke. First measurement of radioisotopes by collinear laser spectroscopy at an ion-guide separator. *Journal of Physics G*, 23:L97–L102, 1997.

[8] *The practical application of light*, chapter Optics guide, pages 2.1–2.12. Melles-Griot, 1999.

[9] M. Shimizu. Lifetime of metastable fluorine atoms. *Applied Physics B*, 72:227–230, 2001.

[10] P. Rhagavan. Table of nuclear moments. *Atomic Data and Nuclear Data Tables*, 42:39, 1989.

[11] J. Yan et al. Systematics of triaxial deformation in Xe, Ba, and Ce nuclei. *Phys. Rev. C*, 48:1046, 1993.

[12] H. Iimura et al. Nuclear moments and isotope shifts of ^{135}La, ^{137}La, and ^{138}La by collinear laser spectroscopy. *Phys. Rev.*, C68:054328, 2003.

[13] R. Delawder. The basics of black oxide. http://www.swdinc.com/black_oxide.htm, 2000.

[14] G. Gerstenkorn. *Atlas du spectre d'absorption de la molécule d'iode*, volume $14800 - 20000cm^{-1}$. Laboratoire Aimé-Cotton CNRS II, 91405 Orsay, France, 1978.